https://doi.org/10.15407/ufm.20.02.213

Yu.S. PROJDAK, V.Z. KUTSOVA, T.V. KOTOVA, H.P. STETSENKO, and V.V. PRUTCHYKOVA
National Metallurgical Academy of Ukraine,
4 Gagarin Ave., UA-49000 Dnipro, Ukraine

REGULARITIES OF FORMATION OF STRUCTURE, TEXTURE AND PROPERTIES UNDER THE COMBINED PLASTIC DEFORMATION OF THE LOW-CARBON AND ULTRALOW-CARBON STEELS FOR COLD PRESS FORMING

The current paper reports the new solutions intended to enhance the complex of mechanical properties and tendency to the press forming of the hot-rolled low-carbon and ultralow-carbon steels with subsequent cold deformation via upsetting and torsion under hydrostatic pressure (THP). Using state-of-the-art research methods, the feasibility of forming an ultra-fine-crystalline structure through the combined plastic deformation is established. The dependence of the change in mechanical properties on the structural and textural parameters as well as phase composition is established. This research is the first wherein the mechanical properties have been determined by the method of nanoindentation for the 08пс, 01ЮТ, 01ЮТ(Ca), 01ЮТА steels, which were initially hot-rolled and afterwards underwent the cold deformation by the THP method. The increase in the indentation hardness by 2 times (5.5–6.0 GPa) is revealed along with the decrease of the modulus of elasticity by 1.5 times (150–190 GPa), but with the opportunity to sustain the satisfactory ductility (δ = 0.75–0.8). This provides a great suitability to the cold press forming of the steels as compared to their initial hot-rolled state.

Keywords: ultra-low carbon steels, nanoindentation, severe plastic deformation, torsion under hydrostatic pressure, press forming, texture.

1. Introduction

The world achievements in the sphere of automobile industry demand that the manufacturers decrease their product weights and lower the production costs but increase the operational safety degree. The most

suitable for these applications are low-alloy steels with conventional mechanisms of strengthening as well as much promising IF-steels (interstitial free steel). Manufacturing volumetric blanks of various metals and alloys with nanocrystalline structures or ultra-fine crystalline structures by means of severe plastic deformation (SPD) is one of the directions being actively developed in the nanomaterials sphere. Among the SPD methods, torsion under hydrostatic pressure and equal channel angular pressing are most widely applied.

The development of the materials with ultra-fine-crystalline structure and the new level of properties via the SPD methods is impossible without the profound knowledge of the regularities according to which the structures change under the treatment regime influence. From the above considerations, it is easily deduced why more and more topical are becoming the researches addressing the development of new steels for automotive sheets in terms of their quality as well as their production technologies. The developments of such kind could be performed if based on grounded fundamental researches and those of the applied nature for the sake of the processes and the phenomena occurring during the manufacturing procedure and further operations with the metal produced. However, the higher strength normally means decrease in ductility for metals. Attaining high strength along with high ductility for developing new promising construction and operation materials is one of the fundamental challenges for the material science. Concerning ultra-fine-crystalline structure metals and alloys, this problem can be solved by means of control over their microstructures.

The influence of the structure fineness on the set of properties in steels is described in the publications of V.V. Rybin, V.I. Trefilov, K.D. Potomkin, Yu.V. Milman, S.O. Firstov, V.F. Moiseiev. Considering the fact that the cold plastic deformation is widely recognized to be the efficient way for strengthening steels, there are publications (by R.Z. Valiev, V.M. Sehal, S.V. Dobatkin, Yu.Ya. Meshkov, M.L. Bernshtein, A.A. Baranov, T.G. Langdon) devoted to the analysis of the structural changes of the metal under deforming conditions, but the information on the influence produced on the structures and the textures of low carbon and ultralow carbon steel is still not comprehensive. Therefore, there is still a true need in the researches aiming at establishing the regularities between the deformation regimes and the properties of thin-sheet rolled stock of low-carbon and ultralow carbon steels, namely their structures, textures, phase compositions and machinability properties.

After the introduction, the second section of this publication reviews the contemporary researches reporting on the methods of plastic deformation for low carbon and ultralow carbon steels, the regularities of their structure formation, their properties, the contemporary interpre-

tation of the deformation process occurring in metals and alloys. The papers addressing the problem of the deformation degree influence on the properties of thereof steels are also regarded in this section. Based on the information obtained from the scientific and the patented sources, the solution stages for this urgent scientific and engineering problem have been determined and they are considered as the development of the rational regimes of combined plastic deformation for the low carbon and the ultralow carbon steels with the purpose to improve their properties.

The third section provides the data on the material and research methods. The object of the research is the samples of the hot-rolled low carbon and the hot-rolled ultralow carbon 08пс, 01ЮТА, 01ЮТ, 01ЮТ(Ca) steels, which are subjected to the additional cold plastic deformation by means of the torsion under hydrostatic pressure.

The fourth section deals with the specific character of the structure formation for hot rolled low carbon and hot rolled ultralow carbon steels subsequently deformed by the methods of torsion under hydrostatic pressure. Here, we report on the materials concerned with the influence of the additional plastic deformation on the sizes of the crystallites, the density of dislocations, the lattice parameters, and microstrength for the investigated steel samples.

The fifth section describes the electronic microscopy studies conducted with thin foil samples of the hot-rolled steels of 01ЮТА, 01ЮТ, 01ЮТ(Ca), 08пс grades. This allows observing the structural changes in the process of combined plastic deformation.

Finally, in the sixth section, the characteristics of the strength and the ductility of the hot-rolled low-carbon and the hot-rolled ultralow carbon steels, which have been subsequently cold deformed, are investigated by the methods of torsion under hydrostatic pressure.

2. Structure, Properties and Methods of the Study for Thin-Sheet Low-Carbon and Ultralow-Carbon Steels for Automobile Industry

2.1. Low-Carbon Construction Steels for Cold Press Forming

The world's automobile industry is dynamically developing and consumes a significant part of the global steel thin sheet production. The products manufactured from these sheets are produced by the methods of plastic deformation (press forming, deep drawing) and they can make up to half of a modern wheel vehicle. The main requirement for sheet steels in drawing is to provide a high degree of formability when the manufacture of the components to possess intricate shapes and high quality surface after the deformation, which is a strict requirement for protective coatings.

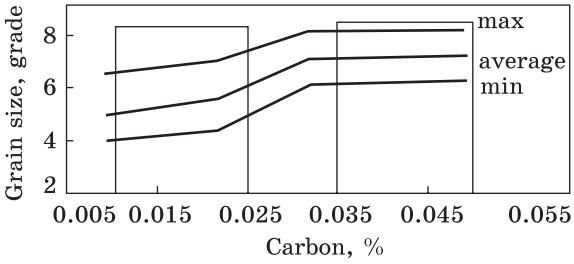

Fig. 1. The effect of carbon content in steel on the grain size of a ferrite in the matrix structure [2]

The high plasticity of the solid parts prevents their brittle fractures in the events of accidents and decreases the weight of the car.

Ferrite is the main phase of low carbon and ultralow-carbon steels of structural type for cold press forming. It undergoes aging during its structural transformations triggered by the manufacturing process and as the result, ductility is reduced but strength is increased. This hampers or even makes it not feasible to carry out press forming by conventional effort of the press, especially when the manufacture of solid parts is commonly performed in two or three operations according to the technology. The process of aging proceeds spontaneously: from the unstable oversaturated state of the ferrite to the maximum equilibrium (natural aging), or because of plastic deformation (deformation aging). For example, low carbon steel at the temperature of 400 °C can contain approximately 0.02% of nitrogen in a solid ferrite solution, but once it is cooled down to 100 °C and rolled, it loses all its nitrogen from the solid solution into the Cottrell clouds. Thus, this steel is capable of aging and actually is not suitable for the manufacture of the car solid parts [1]. Further, in order to prevent the deformation ageing of steel, the carbide-forming and nitride-forming elements are introduced into its content; it is aluminium in priority that is able to neutralize the harmful effects of excessive C and N. Furthermore, the steel acquires non-ageing properties and is assigned 08Ю grade. If the increased strength is required, it is achieved by doping with phosphorus or with other elements and this is marked as 08ЮП steel grade. This steel is demanded by the automobile plants and meets the requirements of ГОСТ (State Standard) 9045-93 [2].

Carbon is known as one of those elements, which greatly changes almost all the properties of sheet steel, and it bears the special effect on its formability. In the case of the carbon content less than 0.03%, the matrix structure is to consist of relatively large ferrite grains that grow after cold rolling during recrystallization annealing in a bell furnace (Fig. 1). The ferrite grains are able to cause surface defect of so-called orange peel during the press forming process when the automobile solid parts being produced. That plays not in favour of the sheet steel quality. The content of silicon in steels of 08Ю grade is not to exceed 0.02% as

the presence of silicon within the metal strengthens it and makes it brittle. Therefore, the production route for the steel with the silicon content within 0.008–0.012% includes controlled deoxidation since aluminium reduces the silicon from the converter slag having entered the teeming ladle before the tapping completion and the ladle refractories are also capable of providing the additional silicon penetrating into steel.

Manganese exhibits both direct and indirect effect on a wide range of properties of low carbon steels. First and foremost, it strengthens the ferrite matrix, which is not desirable in 08Ю steel. However, alloying with manganese is necessary for binding sulphur into the sulphides, thus preventing the formation of the defect of the so-called band structure during the hot rolling operation. Moreover, manganese has a noticeable effect on the kinetics of steel aging, as it slows down the rate of nitrogen coming off from the ferrite lattice.

Thanks to the above-said influence produced by manganese on steel, manganese amounts introduced into steel are to exceed by 10–15 times the sulphur content and are commonly within the range of 0.17–0.21%.

Similar to sulphur, phosphorus tends to worsen the ductility of low-carbon steels and its content is required to be limited to meet the appropriate standard demand.

The character and the degree of the interconnection between aluminium and nitrogen in 08Ю steel have a powerful influence on the capability of low carbon steel for deep drawing and to extra deep drawing, that is, formability without defects on the automobile solid parts.

Aluminium is introduced into steel with the purpose to remove that oxygen from the melt, which enters it during the period of tap-to-tap time and tapping. At the same time, aluminium interacts with nitrogen

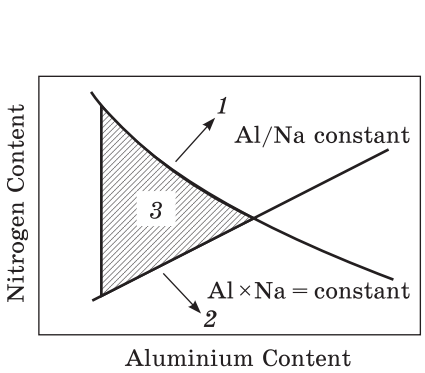

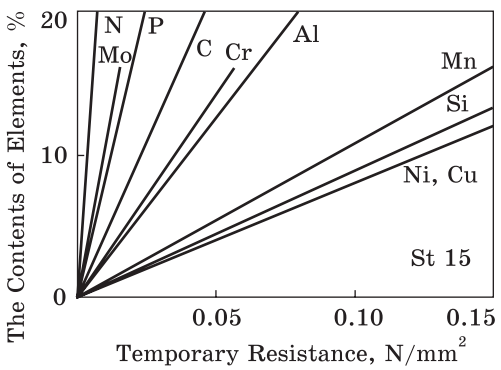

Fig. 2. Schematic representation of the virtual compromise between the aluminium and nitrogen contents in the sheet steel for an extra deep drawing [4], where *1* — increase of the yield strength and temporary resistance, *2* — fine grain, *3* — working area

Fig. 3. The effect produced by low contents of chemical elements on the temporary resistance of cold-rolled annealed steel intended for deep drawing [4]

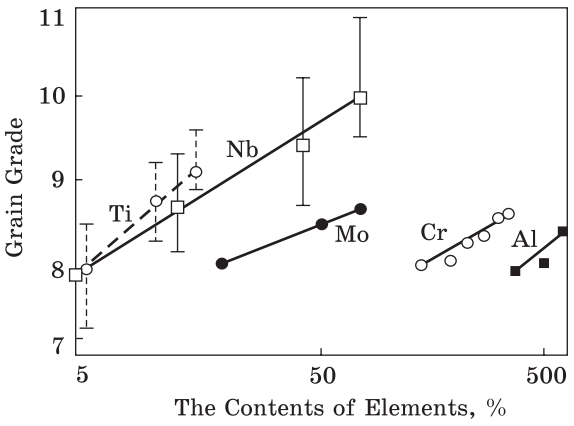

Fig. 4. The influence of low contents of chemical elements on the ferrite grain size within cold-rolled strips after annealing in a bell furnace [4]

dissolved in the ferrite and forms the nitrides, which are released in the form of dispersed particles. This inhibits the growth of ferrite grains during recrystallization annealing operation and strengthens steel but insignificantly. By facilitating the removal of nitrogen from the ferrite lattice, aluminium even at the stage of the molten steel heat production eliminates the possibilities for this steel to undergo deformation aging at deformation and heat treatment.

Nitrogen content decreasing in steel is a way to reduce the yield strength, which contributes to the formability of the thin sheet steel. At the same time, it is a way to decrease the anisotropy of the thin sheet structure and properties, to decrease the normal anisotropy coefficient (r), which complicates the metal forming for the vehicle parts [3]. The appropriate amounts of aluminium introduced into that steel which contains the predicted or measured amounts of nitrogen are the path of a tried and tested compromise capable, as well as whatever compromise does, of partial forming a satisfactory sheet formability. An example of the virtual compromise is schemed in Fig. 2. The content of nitrogen in 08Ю steel does not normally exceed 0.006–0.007% on condition that the cold-rolled metal is to be subjected to annealing in a bell furnace.

If the annealing of cold-rolled strips is carried out on continuous lines, the steel is to contain less than 0.004% of nitrogen. According to the recommendations for the cold-rolled strips passing the annealing operation in bell furnaces through their production route, the aluminium content for introduction into the molten metal is to be 5 times more than the content of its nitrogen. While the aluminium as much as 10 times nitrogen content is to be observed if annealing is of a continuous type (at least one third of aluminium is consumed for binding the oxygen of the melt and subsequent oxide formation).

Optimally, the content of the dissolved aluminium within low-carbon steel of 08Ю grade is to be within 0.03–0.04%, in accordance to the technology adopted in a steelmaking shop.

The chemical elements, introduced into the melt by means of the charge constituents (iron, scrap, casual additives), except those intro-

duced into the charge calculation, are able to influence drastically both the mechanical properties and the microstructure of the rolled products made of 08Ю steel.

The character and the degree of this effect are shown in Figs. 3 and 4. The majority of the chemical elements can be considered as those which strengthen the solid solution during recrystallization annealing carried out for cold-rolled low carbon steels in bell furnaces as the prolonged treatment of the rolled stock is inherent to them, providing the structure state and the stress level close to the equilibrium. This is mostly expressed for phosphorus, weaker for manganese, silicon, copper and nickel.

No less pronounced is the influence of various elements on the grain size: niobium and titanium are the most strong ferrite grain refiners while molybdenum and chrome are less effective in this.

The above data allow us to conclude that in order to achieve the required properties of 08Ю steel, we have to maintain the minimum contents of the elements for solid solution strengthening (phosphorus, manganese, silicon, copper and nickel) and control the contents of the elements affecting grain size (niobium, titanium, chromium and molybdenum). In addition, we have to coordinate carefully the content of the elements that contribute to the formation of the particles of carbides, nitrides, carbonitrides [5, 6]. Thus, the very low contents of the mentioned elements are an important prerequisite for the production of 08Ю steel suitable for thin sheets, capable of deep formability. In this case, the steel is to contain miserable amounts of nitrogen and the aluminium amounts corresponding to them.

The national standards do not limit the contents of nitrogen, chromium, nickel, copper, molybdenum, titanium, vanadium within 08Ю steel. However, the metallurgical plants utilizing their many-year experience in the production of thin sheet steels with good formability properties establish the requirements for the contents of those chemical elements, which are non-standardized for 08Ю steel. As an example, can serve the fact that in low-carbon steels for automobile industry, the chromium content should not exceed 0.03%, while copper and nickel should not exceed 0.06%. The weight content of niobium in steel is not to exceed 0.005%, while titanium is to be within 0.003%. Molybdenum and vanadium are allowed in an amount not more than 0.01% each of them.

2.2. The Automotive Steel without Atom Introduction into Ferrite Lattice

The quality of cold-rolled products made of low-carbon thin sheet steel of non-aging type do not satisfy the increased market demands of the XXI century for automotive metal. The development of new steels should

meet the goals of the new century, the rhythm of its fast life, high speeds of movement, the necessary degree of the safety and the environmental friendliness [7, 8].

The IF steels are widely applied for their rather high strength and sufficient ductility, their application enables the decreases in the automobile weight, fuel consumption, and carbon dioxide exhaust. From year to year, the technological process of their production is being improved. The plastic anisotropy of the cold-rolled sheet invariably increases. The coefficient of the normal anisotropy for the cold-rolled sheets for some grades of steel has increased to $R = 2.2–2.4$ [9].

Thin sheet steel used in automobile construction, can be divided into three groups: conventional steels for cold press forming (yield strength <210MPa, tensile strength <340 MPa); high strength steel (yield strength >210 MPa, tensile strength >340 MPa); high-specific-strength steels (yield strength >550 MPa, tensile strength >750 MPa).

Both cold-rolled and hot-rolled pickled automotive sheet steels are usually supplied in a relatively narrow range of thicknesses (0.5–4.0 mm) with appropriate quality indicators, which are intended for the manufacture of specific parts, knots and car panels. The quality of automotive steel is evaluated, above all, by its formability, strength, degree of the destruction energy absorption, elastic modulus value, and ability to perceive the process of parts connecting with a laser beam, reliability of the adhesion of its surface with paint and corrosion resistance.

The composition and the level of car sheet quality parameters determine the use of appropriate steel grades for internal and external solid panels (IF, VH, DP, SR), for passive safety elements (HSLA, TRIP) and for the manufacture of bearing units and power components (Mart, MnB). In Ukraine, there have been no class of IF until recently, this is explained by the absence in a steelmaking shop equipment feasible to provide an appropriate system of technologies for these type of steel (steel heating, secondary metallurgy and steel teeming). Currently, PJSC Alchevsk Iron & Steel Works is building a modern converter workshop with two 300-ton converters of combined blowing. The station for pig iron desulphurisation in the mixers is foreseen within the converter shop. However, even presently steel is there produced in twin-bath steelmaking units with a capacity of 2×300 t, is refined at a ladle furnace and VD/VOD, and is cast at two-strand slab continuous casters.

The relative amounts of microalloying elements (titanium and niobium) to be introduced into steel depend on the actual contents of carbon, nitrogen and sulphur in the melt and are determined by the calculations as follows. (a) For steels microalloyed with titanium: $Ti = (4C + 1.5S + 3.43N)\%$. (b) For steels, microalloyed with titanium and niobium: $Ti = (2.4S + 3.43N)\%$; $Nb = 7.75C\%$. The deviation in the titanium content is allowed to be $+0.03\%$, while that in niobium content of $+0.02\%$.

2.3. Methods of Processing Automotive Thin-Sheet Low-Carbon and Ultralow-Carbon Steels

2.3.1. Technologies of Hot Rolling and Cold Rolling, Thermal Processing of Thin Sheets from Automotive IF-Steels

The required characteristics of a thin sheet IF-steel are developed predominantly at the stage of the controlled rolling technique at a broad strip hot rolling mill. Its temperature regime and force conditions of metal deformation are determined during the experimental rolling processes for the experimental strip lots. Moreover, the main attention here is paid to the experimental determination of the optimal heating temperatures for slabs, the concluding stage of rolling and the operation of a strip rolling into a roll. These temperatures are interrelated with the amounts of microalloying steels with Nb or Ti or both and at the same time with numerous mechanisms of structure formation (niobium the predominantly responsible for this). (1) During the inhibition of the recrystallization process and consequent refinement of the matrix grain with Nb*X* particles, which despite their significant dissolution in γ-iron lattice at slab heating, partly precipitate again under thermal mechanical effect of the rolling process. (2) The polymorphic transformation, strengthening of steels with the dispersion phenomena, heterogeneous diffusion, which does not develop completely due to atomic radius unsuitability (the atomic radius of niobium is large if compared to that of iron).

We cannot emphasizing the role of Nb in the matrix grain size formation, since the recrystallization process is retarded by the carbonitrides of the microalloying elements, released from the solution during hot rolling and subsequent cooling of the IF-steel strips on the reverse roller of a broad strip hot rolling mill.

The microstructural processes in IF-steels often overlap with each other in time and have a mutual effect on each other. They occur at the time when a slab is in a furnace as well as when the slab is in the roughing group of the broad strip hot rolling mill, and when the broad strip is in the finishing group or on the reverse roller. During these processes, the concentration of the solid solution increases while the grain size decreases, the matrix is undergoing strengthening by means of solidification, the structure transformation regions and those of the phases are expanding, which have a cumulative effect on the entire set of properties of the finished rolled metal.

By the targeted change in the process parameters of IF-steel hot rolling, one can control the microstructure that means producing sheets with the necessary mechanical properties, texture and anisotropy, namely, the control over the steel formability.

The temperature regime for hot-rolled strips (produced from IF steels) is commonly developed for a possibility and necessity to obtain

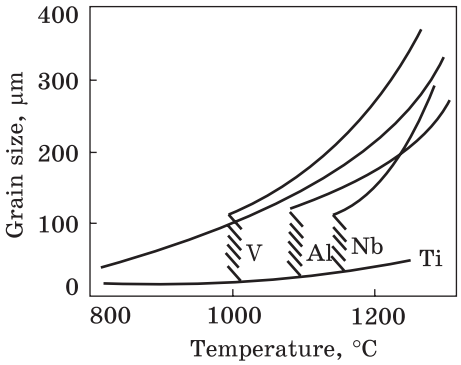

Fig. 5. The dynamics of austenite grain growth at heating microalloyed steel [18]

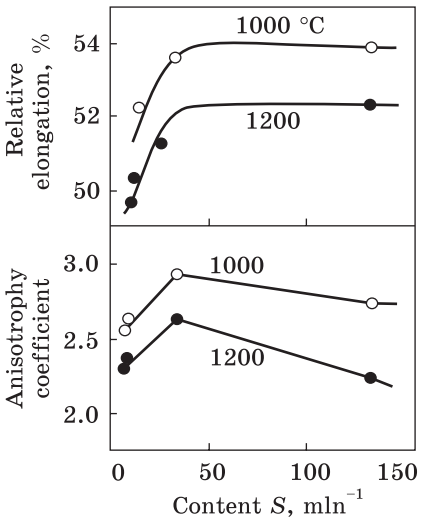

Fig. 6. Properties of annealed strips (at the estimated length of test samples, 50 mm) and heating temperature of slabs [11]

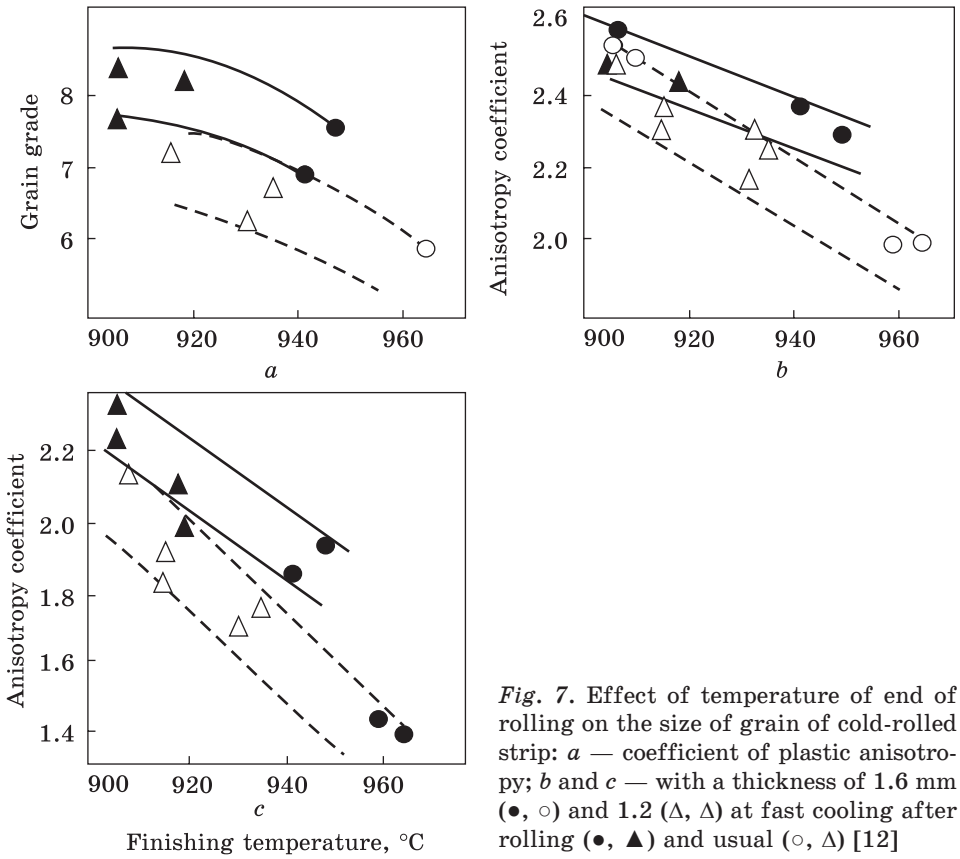

Fig. 7. Effect of temperature of end of rolling on the size of grain of cold-rolled strip: *a* — coefficient of plastic anisotropy; *b* and *c* — with a thickness of 1.6 mm (●, ○) and 1.2 (Δ, Δ) at fast cooling after rolling (●, ▲) and usual (○, Δ) [12]

the metal with a relatively fine grain microstructure of the ferrite matrix. This is facilitated by its microalloying to inhibit the growth of the austenite grains during preheating the dedicated slabs for rolling operations. The degree of ferrite grain growth restrain is illustrated by the curves in Fig. 5.

In accordance with the graphs, that type of Ti that forms resistant nitrides at the crystal boundaries at steel heating, retards austenite grain growth most intensively. The relatively low speed of austenite grain growth occurs in case of steel heating to the temperature not exceeding 1000 °C. The anisotropy coefficient (r) and relative elongation (δ) are noticeably higher after cold-rolled strip annealing than that of the strips rolled from the slabs and heated to the temperature of 1200 °C as it is implied by the data in Fig. 6. However, force and energy conditions of hot rolling for strips predetermine the necessity of heating IF steels slabs to the temperatures of 1180–1210 °C.

The finishing temperature of strips rolling, the rate of their cooling on a rolling mill roller table and the coiling temperature produce a noticeable effect on the finished steel properties. The degree of this effect can be calculated by the curves in Fig. 7.

2.3.2. Severe Plastic Deformation. Structure Formation at SPD of Steels

The processes of obtaining submicrocrystalline and nano-microcrystalline materials (with grains size less than 1 μm and less than 100 nm) by means of plastic deformation are often called by the generic term of SPD. The severe plastic deformation technique involves compression with high degrees of deformation along with the application of high-pressure values at the temperatures less than the temperature of recrystallization [13, 14]. Y.E. Beygelzimer introduces the definition [15] of strain accumulation processes, which occur at SPD. Their main goal is the accumulation of strain in the blanks, but not their shape change. When preparing nanocrystalline structures, the obtained level of the true degree of strain can reach 4 and more. In order to describe these processes, it is suggested to use the term of megaplastic deformation. Obtaining bulk nanostructured metals and alloys via SPD becomes an important rapidly developing branch of the contemporary material science. This process is aimed at creating materials with high mechanical and physical properties. The dispersion of a microstructure to a submicrocrystalline or nano-microcrystalline level causes a significant increase in strength, in fatigue strength and a decrease in the transition temperature into the material superplastic state [15, 16].

The most popular techniques of SPD include high-pressure torsion (HPT), based on the Bridgman anvil method and equal channel angular pressing (ECAP), the latter was suggested by V.M. Segal in 1972 and further developed by Valiev [17].

The principal effect of ultra-fine-crystalline structure in the materials after SPD is the increase in the final material strength due to the refining initial coarse-grained texture. The experimental results in Refs. [18–22] confirm the possibility of applying SPD methods to both readily deformed materials and many difficult-to-deform ones. Among the peculiarities of the final structure, one can obviously distinguish a fine grain size, predominantly high-angle boundaries with disordered structural elements, a low density of the dislocation inside the grains and non-equilibrium grain boundaries. With the objective to understand the processes of structuring during severe plastic deformation, the large-scale studies of the single-phase materials as well as the materials with a small quantity of the second phase [23–27] have been carried out. In accordance with these studies, two main mechanisms of grain refinement during SPD have been defined. The first mechanism is based, first of all, on the dislocation activity, that is the accumulation of the dislocations, their interaction and spatial rearrangement. This results in the refinement of the coarse grains into numerous fine grains by forming dislocations, and the evolution of the boundaries with a low angle of disorientations into those with the high-angle grain boundaries [28–29]. In the course of structuring within the areas of high density of the dislocations, there occurs the arrangement of the dislocations into the dislocation 'walls', which transform into deformation bands at deformation degree increasing [29]. The dislocation walls surrounding the regions with a relatively low dislocation density form a cellular structure. The peculiarities and the physical form of such structures depend on the material and are determined by the stacking-fault energy (SFE) and the degree and temperature of deformation. When the temperature increases, the thickness of the dislocation walls decreases until the subgrain boundaries formation and, accordingly, the number of the internal dislocations decreases. The deformation degree affects the size and the disorientation of the adjacent cells: the increase in the deformation degree leads to the decrease of the average cell size but the increase in the angle of the disorientation between the adjacent cells.

The second mechanism of structuring during SPD, where the deformation of twinning dominates, is commonly observed in f.c.c. metals with low stacking-fault energy, for example, in TWIP steels [30, 31], Cu–Zn [43] and Cu–Al alloys [32, 33]. The mechanisms of deformation twinning have been studied widely enough. Several mechanisms of the deformation-twins' formation have been suggested for f.c.c. materials in Refs. [34–39]. Information that is more detailed is provided in the review paper [40].

Wang et al. [41] have noted that not only the primary, but also the secondary deformation twinning is characteristic of the second mecha-

nism of grain refinement in the process of SPD. This deformation twinning refines coarse f.c.c. grains by means of the interaction between the dislocations and the twins' boundaries, thus transforming the twins' boundaries into conventional high-angle grain boundaries. In publication [41], it is reported that the minimum achievable grain size is determined by the minimum thickness of the twins. It is known that the average thickness of a twin in the highly deformed materials is the function of the stacking-fault energy of material [41]. Obtaining a twin thickness less than 2 nm in the material with low stacking-fault energy is feasible [42]. However, until now, grain size of less than 10 nm has not been obtained. This indicates the great complexity of the grain refinement process in those f.c.c. materials where the stacking-fault energy is even lower than that described by Wang for the Cu–Zn alloy [43]. Moreover, there have been cases registered wherein deformation produced not only the effect of twinning, but also untwining [43–48].

Additionally, the deformation temperature effect on the mechanism of structuring during deformation should be specified. The cross slip and the dislocation mobility require thermal activation. However, the twinning phenomenon during cold working can appear to be more beneficial than the dislocation mobility. Therefore, the structuring mechanisms can be different even at the deformation of the same material if the deformation temperatures are different.

2.3.3. Torsion under Hydrostatic Pressure as One of the Main SPD Techniques. Structuring and Mechanical Properties of Steels during THP

The basic deformation during torsion under hydrostatic pressure (THP) technique is produced due to the torsion of a sample. The applied uniaxial pressure, which usually reaches several GPa, plays two roles. Firstly, the pressure creates a quasi-hydrostatic compression region in the central part of the sample, which prevents its destruction. Secondly, it increases the friction between the strikers and the sample. Due to the high friction, the sample transmits the moment of torsion from the moving striker and the latter is deformed by torsion.

Currently, THP is commonly used for the studies of the SPD physics. At room temperature or at lower ones, THP is applied for producing nanocrystalline structures in metals, alloys, intermetallics and ceramics. The sizes of the samples before deformation are commonly less than 20 mm in diameter and 1 mm in height. After the deformation, the height of the sample decreases down to 0.2–0.5 mm. The significant refinement in the structure is already observed after one-half turn deformation, but in order to create a uniform nanostructure there, as a rule, the deformation of several turns is required.

The THP of pure metals leads to formation of an equated structure with the average grain size of 50–100 nm. In the alloys, the grain size can be much smaller. The mechanism of severe deformation depends on many factors, particularly, on the crystal lattice type and the stacking-fault energy. A strong phasic character characterizes the process of nanostructure formation.

In the pure f.c.c. metals, with a high stacking-fault energy (Cu, Ni), the sequence of structural transformations is as follows. While the torsional deformation increases up to $n \approx 0.1$ (where n is the number of turns of the mobile striker), the dislocations are concentrating within the boundaries of the subgrains (centres), which are almost dislocation-free grain regions of arbitrary form separated from the other regions by low-angle boundaries. At the further increase in deformation up to $n \approx 1$, the sizes of the subgrains are decreasing, and the degree of their disorientation is increasing. At that, there occurs a gradual transition from the subgrain structure into the grains, which mainly contain high-angle grain boundaries.

The severe plastic deformation of alloys together with the formation of nanostructures can also cause the formation of metastable states, for example, the supersaturated solid solutions and the metastable phases. In intermetallic compounds after THP, there can be observed the long-range order destruction that can lead to the complete disordering.

The materials obtained by THP are characterized by a high level of internal stresses and significant crystal lattice distortions. In such materials, there can be found the anomalies of some fundamental properties, for instance, elastic moduli, the Curie and Debye temperatures, saturation magnetization. As a rule, the materials obtained by THP are characterized by the high strength at relatively low temperatures, high plasticity and superplasticity at elevated temperatures.

The scheme of a contemporary plant for processing by the method of torsion under hydrostatic pressure described in Refs. [49–54], is shown in Fig. 8. It differs from Bridgman anvil [55] by a deepening in the lower bar of the plant. It prevents metal creeping, which results in providing quasi-hydrostatic pressure that allows the samples to be deformed for a long time without destruction. When the lower anvil is rotating, the sample is being deformed by a non-precision offset owing to the surface friction.

The deformation degree produced by THP can be calculated by the formulae presented in Ref. [55]. The same formulae have been used in the earlier studies for Cr–Ni steels [56] and f.c.c. metals [57] after THP.

The first important results of these studies are obtaining an average grain size of d_{av} less than 100 nm under THP (P = 6 GPa, ε = 7.1), the decrease of d_{av} with the decrease of stacking-fault energy [58], the possibility of a low-temperature recrystallization of nickel and copper sin-

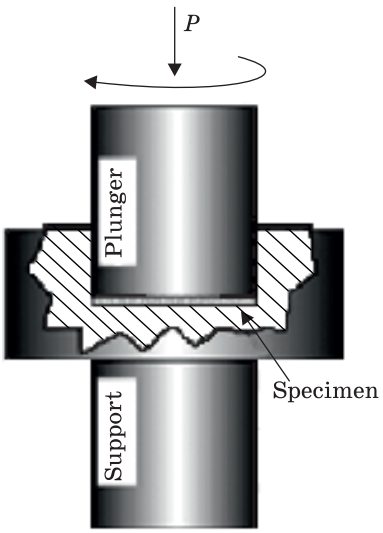

Fig. 8. Scheme of severe plastic deformation (SPD) of torsion under hydrostatic pressure (HPT) [57]

gle crystals, which have been deformed by THP (ε is more than 5) at the temperature lower than the homologous temperature of $\propto 0.4T_{\text{melting}}$ [58], and the possibility of phase transformations in Fe–Ni alloy caused by THP (at P = 8–10 GPa $\varepsilon \approx 5$) [59]. To obtain this effect under static compression it would be necessary to apply a load of about 20–22 GPA.

Shear in the centre of the sample equals zero and increases with the radius extension, provided if the thickness of the workpiece remains constant. However, the close values of microhardness at different points indicate that the structure in the centre of the sample is refined in a way similar to those in the other areas of the radius [60–62]. The disalignment of the strikers or other deviations from the ideal THP scheme may be the reason why the area of the reduced microhardness disappeared within the sample centre [63]. Moreover, during THP, the initial sample thickness somewhat decreases after deformation, and the use of the initial thickness data in the formula makes the estimated value of deformation lower as compared with the true value. In actual practice, the calculation formulae can be considered as only approximately equal to the actual deformation degrees. Additionally, it should be taken into account that the nanocrystalline structure is formed under the influence of not only external stresses, but also internal ones as well, that are not related to the true deformation. The THP method provides rather high-applied stresses for obtaining practically homogeneous structures with the maximum refined grain [64–67].

In the early publications (see Ref. [68] and references therein), the sequence of structural transformations in THP process has been studied with such materials as Ni, Cu with the f.c.c. lattice and the high stacking-fault energy. Based on the obtained results [68, 69], the following phasic model of structuring has been proposed. The first stage of the reinforcement is characterized by the higher density of dislocations that rearrange in the boundaries of the cells with the higher deformation. Their sizes stabilize at the value less than 1 μm when reaching the deformation ε = 1.5–2. Further, with deformation ε = 2–4, the process is characterized by the dislocations accumulation in the cell boundaries. One can observe an increase in the angles of the cell boundaries disori-

entation up to the angles of approximately 10°. When embedding the dislocations into the subboundaries exceeds the possible limits, the further accumulation of dislocations inside the cell begins, which is accompanied by mechanical reinforcement at $\varepsilon = 4–5$. Under conditions of THP, the high level of internal stress causes the formation of the high-angle boundaries with disordered structural elements, which serve as a warehouse for a large number of excessive dislocations. This expression of rotational deformation modulus extends over the whole sample and the deformation acquires the stable stage.

The study of the armco iron in Ref. [70] confirms the stages of nanostructures formation under the torsional severe plastic deformation. At the first stage, with deformation N from 1/4 up to 1 turn, a cell structure appears with low-angle boundaries, disordered structural elements and a cell size of about 400 nm. Further, at the second stage, which proceeds from 1 turn to 3 turns, the transition structure with the signs of a cellular and a granular one is formed. With the increase in the deformation degree, an average size of cells decreases, while the angles of boundaries disordering increase, evolving gradually into a homogeneous ultra-fine grained structure of granular type at the third stage. Furthermore, the lattice of grains at the third stage is strongly deformed, because of distant stresses from the non-equilibrium grain boundaries with a high density of grain boundary dislocations.

The electron-microscopic studies after THP procedure carried out for [70] have revealed the similarity of the nanostructure formation stages in the armco iron, in the single-phase steels of 13X23T and AISI 316L grades. The only difference between them is the formation of the finer grains in the steels at the third stage. Thus, it can be stated that the process of structuring under THP has common features for pure metals and alloys.

Ivanisenko et al. [71–74] observes a similar nanostructure formation, as well as the dissolution of pearlite plates in the industrial pearlite steel (≈ 0.7% C) under THP operation. After the shear that equals 100 at room temperature, the sample microstructure has been developing into the cell structure and contains partially dissolved cementite plates. The further increase in the shear up to the level of 200 leads to the nonhomogeneous grain structure formation. During this deformation, the grains of 100 nm in length and 15 nm in thickness have been obtained. The dislocation walls separate the elongated grains with the high density of dislocations. During the deformation, the distance between the cementite plates is reducing. After the shear that equals 300, there develops a homogeneous nanostructure with the grain sizes of about 10 nm and complete cementite dissolution. However, in the alloy of ХН77ТЮР with low stacking-fault energy [75] of disordering, the cell structure has not been formed even at very high degrees of defor-

mation. The structure refinement occurs with the emergence and spread of the shear bands, which with the increase in deformation are filling the whole sample. For the stable deformation stage of $\varepsilon \geq 5$, the structure with the regions that practically do not contain dislocations or high-angle disordering is found to be characteristic. The sizes of the structural elements decrease with the decrease in the stacking-faultenergy.

In Ref. [76], the structural changes of the ferrite and the austenitic steels during the torsion under hydrostatic pressure (THP) at room temperature have been investigated. With the equivalent strains that are equal to $\varepsilon_v = 8$ and $\varepsilon_v = 32$, the publication reports on obtaining a microstructure with an average structural element size less than 100 nm. On comparing the obtained results with the armco iron, the austenitic and the ferrite steels, it has been shown that the refinement of the initial grains into the small crystals within the structure in case of both steels has been shifted toward the lower deformation degrees. Any significant changes have not been noted for equivalent strains above $\varepsilon_v = 16$ for steel, but the sizes of the structural elements are less than in the armco iron. The publication [76] has concluded that the grain size reduction is conditioned by the increase of the alloying elements number as well as the decrease in the stacking-fault energy. Both factors are clearly defined for these steels.

The research reported in Ref. [77] presents the results with the ultra-fine grained structure formation in carbon steels of 20 and 45 steel grades under torsion in SPD at certain pressure and the temperatures of 20 and 400 °C. It has been shown that an almost homogeneous structure with crystal sizes of 100–200 nm forms in both steels at room temperature, while at elevated temperature the deformation localization occurs in the sample periphery along with the formation of the nonhomogeneous microstructure in its diameter. SPD by torsion leads to the increase in the material microhardness, the microhardness value after deformation carried out at 400 °C is 2.5 times higher than that after the deformation at 20 °C.

Thus, SPD with carbon steels of 20 and 45 grades causes the formation of the nanocrystalline structure with the grain or the fragment size of 100–200 nm. During SPD by torsion, the nonhomogeneous deformation occurs, the degree of inhomogeneity of this deformation increases towards the peripheral area of the samples.

The deformation degree localization increases with the increase in deformation temperature. However, despite the microstructure inhomogeneity, which can be detected by the optical metallography, the electron-microscopic research shows the refinement of the grains across the diameter of the samples both on the periphery and in the central sample area. It should be noted, that the increase of the deformation temperature does not lead to the increase in the sizes of the fragments, though

they have non-equilibrium boundaries, capable of the offset or migration [78–87]. Probably, this deformation scheme with the shear component predominance does not ensure any conditions for the grain-boundary and the fragments migration that could lead to an increase of their sizes. The other factor to prevent the growth of the grains could be the disperse carbide particles that cause Ziner inhibition [87].

Thus, the structuring process is staged at THP and the average size of the structural elements depends on the parameters of deformation as well as on the material itself and its chemical composition.

3. Research Materials and Methods

3.1. Materials

As the research materials, we selected the sheet metal cards of 2.07 mm thick made of 08пс steel grade and rolled on a continuous sheet rolling mill 1680 at the industrial plant of open joint stock company Zaporizhzhya metallurgical plant 'Zaporizhstal' (Ukraine, Zaporizhzhya). The samples of 01ЮТА, 01ЮТ, 01ЮТ(Ca) steels were taken from the cards with 3.5 mm of thickness after hot rolling on the continuous hot-strip mill 2000 and pickling on the continuous pickling line, both operations conducted at the industrial shop at the open joint stock company 'Lipetsk metallurgical works' (Russia, Lipetsk). The chemical composition of the studied steel grades is given in Table 1.

3.2. Methods

The experimental studies on the temperature rolling conditions were carried out in the rolling laboratory of the Institute for Ferrous Metallurgy named after Z. I. Nekrasov of the National Academy of Sciences of Ukraine. Table 2 presents the rolling deformation modes for the studied grades of steel. The procedure of the samples' preparation is as follows. Metal heating before rolling was conducted in electric furnace СН 1.62.51/11-И2 at the rate of 3 °C/s and holding time of 2–4 seconds. The rolling was carried out on the laboratory single stand double-high mill 280 in one or two passes (at the rolling speed of 1.4 m/s, the pause between the passes made up the interval of 13–15 seconds). After rolling, the cards of steels underwent air-cooling (from the temperature of the rolling completion to the ambient temperature ($V_{\text{cooling}} \approx 5$–$8$ °C/s). In order to simulate the process, the coil was charged into electric furnace of 25414/11-И1 type, where the temperature corresponded to the coiling temperature, and it was cooled along in the furnace to the ambient temperature ($V_{\text{cooling}} \approx 0.05$ °C/s).

The severe plastic deformation for the samples was carried out through the method of torsion under hydrostatic pressure on the plant similar in

its type to the Bridgman anvil; the experiment supervision was conducted by the head of the Department of Technological Engineering V.F. Balakin, doctor of engineering science, professor at the National Metallurgical Academy of Ukraine. The samples had been subjected to cogging at room temperature by compression and then by torsion to different degrees of deformation.

After hot rolling, the low carbon and the ultralow carbon steels were subjected to the additional plastic deformation by torsion under hydrostatic pressure (see Table 3).

The true deformation under torsion has been estimated by the following formulae according to publications [88–92]:

$$\varepsilon = \ln\left(\frac{\varphi r}{h_1}\right) = \ln\left(\frac{2\pi N r}{h_1}\right), \qquad (3.1)$$

Table 1. **Chemical composition of low-carbon and ultralow-carbon steels**

Steel grade (type)	Chemical composition, wt.%											
	C	Mn	Si	P	S	Cr	Ni	Cu	Al	Ti	N_2	Ca
01ЮТА	0.002	0.12	0.01	0.006	0.011	0.01	0.01	0.02	0.05	0.062	0.005	0.0002
01ЮТ	0.003	0.13	0.02	0.008	0.012	0.01	0.01	0.02	0.041	0.056	0.004	—
01ЮТ(Ca)	0.003	0.12	0.01	0.005	0.011	0.01	0.01	0.02	0.041	0.070	0.004	0.0003
08пс	0.080	0.30	0.01	0.023	0.030	0.04	0.03	0.03	0.020	—	—	—

Table 2. **Rolling deformation modes or 01ЮТА, 01ЮТ, 01ЮТ(Ca), and 08пс steels**

Steel type	$T_{heating}$	$T_{1rolling}$	h_0	h_1	Δh_1	ε_1	$T_{2rolling}$	h_2	Δh_2	ε_2	$\Sigma\Delta h$	$\Sigma\varepsilon$	$T_{cooling}$
	°C		mm			%	°C	mm		%	mm	%	°C
01ЮТА	1000	970–980	3.5	1.8	1.7	48.6	730–740	1.30	0.50	27.8	2.2	62.9	660–680
01ЮТ	1000	970–980	3.5	1.80	1.70	48.6	730–740	1.35	0.45	25.0	2.15	61.4	660–680
01ЮТ(Ca)	1000	970–980	3.5	1.8	1.7	48.6	730–740	1.40	0.40	22.2	2.10	60.0	660–680
08пс	1000	750	2.07	1.9	0.17	8.2	—	—	—	—	—	—	—

N o t e: Here, $T_{heating}$ denotes the sheet steel heating temperature, $T_{1rolling}$ and $T_{2rolling}$ are the temperatures of the steel sheet rolling in the first and second passes, h_0 is an initial thickness of the sample, h_1 and h_2 are the thicknesses of the sample after the first and second passes, Δh_1 and Δh_2 are the metal reductions in the first and second passes, Σh is the total metal reduction in two passes, ε_1 and ε_2 are the relative degrees of the metal deformation in the first and second passes, $\Sigma\varepsilon$ is the total degree of the metal deformation in two passes, $T_{cooling}$ is a coiling temperature

$$\varepsilon = \ln\left(h_0\left(1+\varphi\frac{r}{h_1^2}\right)\right), \tag{3.2}$$

where r is the sample radius (mm), N is the turning number, h_0 is the sample height before the test (mm), h_1 is the sample height after the test (mm), φ is the rotation angle (radian).

The following formula is applied to calculate the shear γ for THP method:

$$\gamma = 2\pi r\frac{N}{h}, \tag{3.3}$$

where N is the turning number, h is the sample thickness, r is the sample radius (mm).

The equivalent strain is used to compare the degree of the shear during THP with the deformation degree at other SPD methods; according to Mises criterion, equivalent strain is calculated by the formula:

$$\varepsilon_{\text{equiv}} = \frac{\gamma}{\sqrt{3}}, \tag{3.4}$$

where γ is the shear.

The nanohardness measurements were performed by means of the nanoindenter G200 (USA) with a diamond triangular Berkovich pyramid. The measurements were made on the depth of 200 nm. The imprints were applied at the distance of 15 μm from each other. Each sample undergone 10 measurements, then the results were averaged. The indentation curve was built to determine the hardness (practically, the load curve) in the coordinate reference system of 'indentation depth–resistance force to the indenter penetration'.

The new indices and characteristics have been introduced into the indentation diagram for the materials mechanical properties and their correlations supplement the existing indices presented in the International Standard ISO 14577 [93]. In general, the method of the automatic indentation provides a practically complete picture of mechanical properties and structural conditions of new contemporary materials of

Table 3. **Parameters of torsion under hydrostatic pressure for the hot-rolled low- and ultralow-carbon steels**

Steel	T, °C	P, kgf/cm^2	P, MPa	h_0, mm	h_1, mm	d, mm	N
08пс	20	155	15.2	0.7	0.5–0.4	9	5
01ЮТА		155	15.2				5
01ЮТ		194	19.02				5
01ЮТ(Ca)		350	34.32				3

Note: T is a deformation temperature, P is a torsion pressure, h_0 and h_1 are the sample thicknesses before and after the tests, d is the sample diameter, N a revolution number

any phase compositions and in any structural conditions even at the smallest samples.

The mechanical properties of the studied steels after THP operations were determined experimentally by the indentation method. The obtained data processing has been carried out by the calculation method using the methodology by S.O. Firstov [94]. The application of the methodology allows defining the indentation hardness, the indentation elastic modulus, the boundary hardness, the non-contact elastic deformation at indentation, the non-contact elastic deformation stress, etc. The methodology enables us to overcome sufficient methodological difficulties connected with obtaining true values for the mechanical characteristics of elasticity, strength and deformation of materials with special properties (including nanostructural materials), the difficulties of such sort arise when the traditional methods of testing are applied.

The characteristics of plasticity for the hot-rolled steels after additional cold working have been determined according to the methodology of Yu.V. Milman [95].

For the studies on the sample microstructures, optical microscopes of Neophot-21 and Nikon Eclipse MA-200 were used and the certain sample preparation procedure was observed. The metallographic samples were prepared in the intersection diametric to the rolling direction using the sand paper (ГОСТ (State Standard) 6456-82 [96]) with consistent reduction of abrasive grit. Polishing with the diamond paste removed the small grooves left after the abrasion and smooth mirror-like surfaces of the metallographic samples were obtained. The polished samples were subjected to etching in the concentrated nitric acid, or to chemical etching in a saturated solution of ferrichloride in chlorhydric acid with the addition of some quantity of nitric acid. The quantitative metallographic analysis has been carried out using the dedicated software for the data processing and data analysis NIS-Elements.

The measurement of the microhardness for the low carbon and the ultralow carbon steels both in the initial hot-rolled state and after THP were carried out via the Future Tech automatic hardness tester FM-700 (Japan) with a load of 500 gf, the microhardness indentation time of 50 seconds, this allowed determining Vickers microhardness. The method of the microhardness measurement is regulated by ГОСТ 9450-76 [97].

The phase composition, the crystal lattice parameters, the crystallite sizes, the dislocations concentration and the microstress values have been studied through X-ray crystallography in FeK_α radiation via ДРОН-3М equipment. The analysis of the shape of the diffraction arcs has been carried out applying the least-squares method and by singling out physical extensions of the lines by the method of the approximations of the line profile by Gaussian [98–102].

The study of the spatial distribution of the structure elements orientations has been conducted via the automatic analysis of the diffraction patterns of the back-scattered electrons (EBSD-analysis) with the application of Kikuchi lines in the scanning electron microscope JEOL JSM-6490 at a 500 times' magnification [102–107]. The abrasion machining and polishing were accompanied by plastic deformation of the surface layers. In order to remove the deformation surface layer of the sample, electrolytic brightening was applied within the chemical agent consisting of 15% perchloric acid +85% acetic acid at the solution temperature of 8–15 °C and under the voltage of 12.5 V. Further, the washing in the distilled water and ethanol followed [108–109]. The automatic determination of the crystallographic orientation on the surface was conducted at steps of 1 μm each; in each experiment, a region of 255×191 steps was chosen and it took 5 hours of the scanning time.

The fine-structural investigation of the low carbon steel samples has been carried out on JEOL electron microscope JEM-100CXII (Japan). The electrochemical polishing was done in the TENUPOL plant in electrolytic conductor: 30 ml of $HClO_4$, 175 ml of *n*-butanol, 300 ml of CH_3OH.

4. The Influence of Combined Plastic Deformation on the Microstructure Formation of Low-Carbon and Ultralow-Carbon Steels

4.1. THP Effect on the Structure Formation of the Hot-Rolled 08пс-Grade Steel

The microstructure of the sheet product determines the level of its mechanical properties and the quality of the pressed parts. The structural components of the hot-rolled low-carbon 08пс steel are presented by soft plastic ferrite and hard brittle cementite. The level of the mechanical properties and the ability of the hot-rolled metal to be drawn mainly depend on the size and the homogeneity of the ferrite grains and on the type and the position of the precipitated cementite [110].

The ferrite grain size in the hot-rolled sheet produced by rolling with the fuel-free mould powder can vary from 7 μm to 35 μm. The fine-grained structure (the grain diameter is 7 μm to 15 μm) increases the strength characteristics and reduces the ductility of the metal that deteriorates its formability. The ductility of the fine-grained steels is lower than that in the steels with the grain of 25–35 μm in diameter while it is 15–20% higher than the ductility of the coarse-grained steel with the grain size of 110–140 μm in diameter [111]. The coarse-grained structure leads to the metal tearing during stamping, and forms a defect of the 'orange peel' on the surface of the pressed parts.

The quality of the hot-rolled products is regulated by the norms of ДСТУ 16523-97, in particular, for thin metal sheets. Accordingly, these requirements to the microstructure are to provide better formability and the necessary quality of the finished parts [112]. Thus, the standard regulates the ferrite grain size, which must not exceed 62 μm for the hot-rolled superfine thin sheet, but the ferrite grain size inhomogeneity is considered acceptable in the boundaries of the three adjacent grit numbers. The high grain-size inhomogeneity leads to the nonuniform metal deformation when drawing, which can cause the metal tearing.

The uniform structure is also necessary in the hot-rolled metal for semi-finished rolled stocks of the cold rolling mills. The favourable structure of the metal appears to be the main prerequisite for achieving the high deep drawing with steels after their final heat treatment, as the hot-rolled metal structure significantly affects the metal structure pattern when it is after cold rolling and subsequent recrystallization annealing. The degree of the metal deformation on the dedicated mills can reach 70–80%, and due to this, the high grain-size inhomogeneity, which worsens the metal formability at cold rolling temperatures, can cause the cracks in the sheets, and, as a consequence, can lead to industrial accidents. At that, the grain-size inhomogeneity is reduced neither by cold rolling, nor by recrystallization annealing [112].

Our research in this section aims at establishing the microstructure formation regularities with regard to the hot-rolled low carbon and the hot-rolled ultra-low carbon steels after severe plastic deformation by THP method at room temperature.

Figure 9 shows the microstructures of the initial blank of 08пс steel: the minimum deformation degree is 8.2% in the region of the ferrite–pearlite metal structure if the heat schedule is up to 750 °C and rolling is carried out in one pass. This provides a uniform texture across the intersection of the complete metal sheet while the ferrite grain sizes are within 8–20 μm (Fig. 9).

The grains are mainly equiaxial. The fine ferrite grain within the steel sheet structure increases its elastic properties, at that the sheet is difficult to form, its surface becomes wavy and resistance to forming increases [114]. The microstructure of the sample under research is by nature a ferrite and a phase that contains carbon in the form of the structure-free cementite in amount less than 10%, which meets the requirements of ДСТУ 5640-68 [115]. The cementite particles with a shape close to a globular one are evenly arranged in the basic ferrite structural component, which appears to be a favourable factor for the hot-rolled metal intended for deep drawing.

In order to increase the mechanical properties and the formability of the hot-rolled 08пс steel, its sample was additionally deformed by THP method at room temperature (refer to Fig. 10 for the images of the

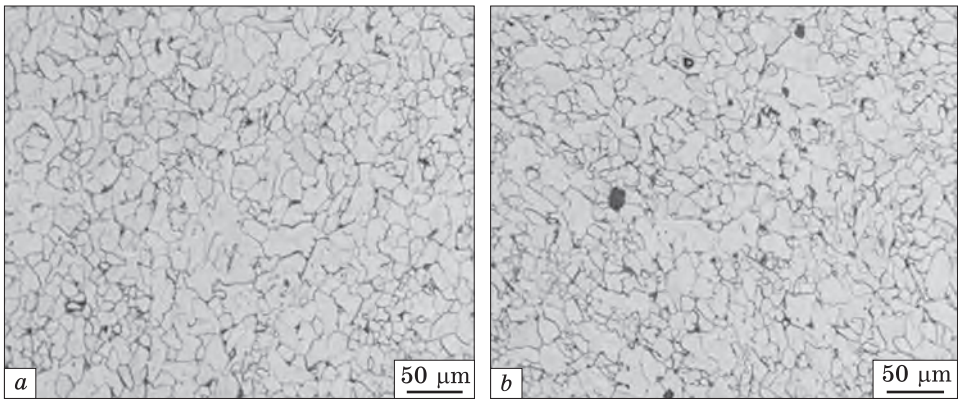

Fig. 9. Microstructure of the hot-rolled 08пс steel, ε = 8% [113]: *a* — surface of the sample, *b* — sample centre

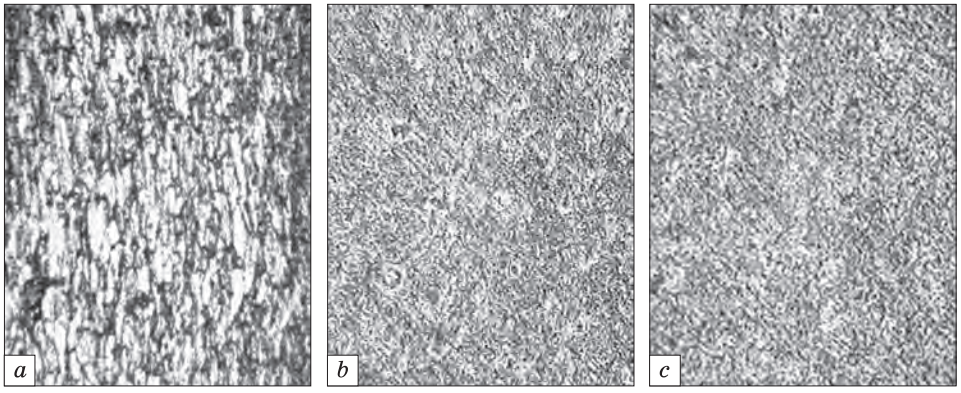

Fig. 10. Microstructure of the surface of the 8пс steel sample after HPT (×250) for e = 1.14 (*a*), e = 2.53 (*b*), and e = 3.16 (*c*) (see also [114–116])

subsequent plastic deformation). The microstructure analysis has showed that after THP of 08пс steel, in the sample centre and in the middle of its radius there is a smaller grain refinement respecting the periphery of the sample, where the maximum grain size decrease with a clear metallographic texture is observed [115, 116].

The shear initiation is a local kinetic structural transition that occurs only in the local area of a crystal due to the phenomenon of the entropy. The subsequent plastic flow in the course of the deformation can be regarded as an absolute relief process, which tends to withdraw the local strong excitation from the volume of the deformed crystal, having used all possible channels of the crystal lattice structural rearrangement. The further evolution determines the regularities of the metal plastic flow, which is a vortex one by its nature [117]. According to the synergetic approach, the convective current appears to be the

most effective channel of the equiaxial system motion to the balance. The crystal being deformed tends to form a structure with the elements capable of conducting a convective current.

An example of such structure can serve the cellular dislocation structure in the crystals with the moderate stacking-fault energy. Each cell moves as an independent structural element, experiencing the translation and the rotational deformation modes. The motion of separate dislocations accommodates interaction of the adjacent cells, during the process of polycrystal deformation, the autonomous motion is active in each grain. At high deformations, the mentioned is clearly expressed. The grain-by-grain mass transfer underlies the structural superplasticity of polycrystals [117]. The condition of maintaining the integrity of the deformed solids determines the multiplicity of the slip in the crystal because of which shear stagnation areas occur. During the deformation, a single crystal is split into the regions with the limited shear stagnation areas, the latter concentrate large stresses and become the regions of the strong excitation that produce defects, i.e., the process of the cross slip develops to determine the crystal behaviour, acting as a structurally nonhomogeneous medium. Thus, during that deformation, which causes the crystal splitting, the following takes place: the regions are formed with the boundaries functioning as the regions of stagnated shears, which are defined by the density of defects and contain powerful stress concentrators. It is commonly known that these regions must accommodate shears that flow on their boundaries while the conditions for the integrity maintenance are not neglected [117]. The classical studies [118, 119] emphasize that when analysing a stressed state of a solid it is extremely important to take into account the shear stress required to create a residual displacement of the solid particles since the effect of the relative shear on the flow often overcomes the influence of the other factors such as normal stresses, anisotropy, etc.

The microstructure study in the sample cross sections has confirmed the presence of the strong deformation localization on the periphery of the samples. Figure 11, *a* clearly shows the metal flow lines in the process of deformation; the lines lead to the clear metallographic texture formation which coincides with the direction of torsion. The plastic distortion of the material is a special form of the mass transfer.

It can occur in a strictly or moderately organized fault motion of the crystal structure connected with the presence of the local excess or the lack of the mass (the interstitials, the vacancies, the dislocations, and their more complex formations). The partial dislocations also satisfy this condition, since they are formed because of the removal or the introduction of the material wedges from the sample or to the sample. Therefore, the motion of the partial dislocations also causes plastic deformation of the material.

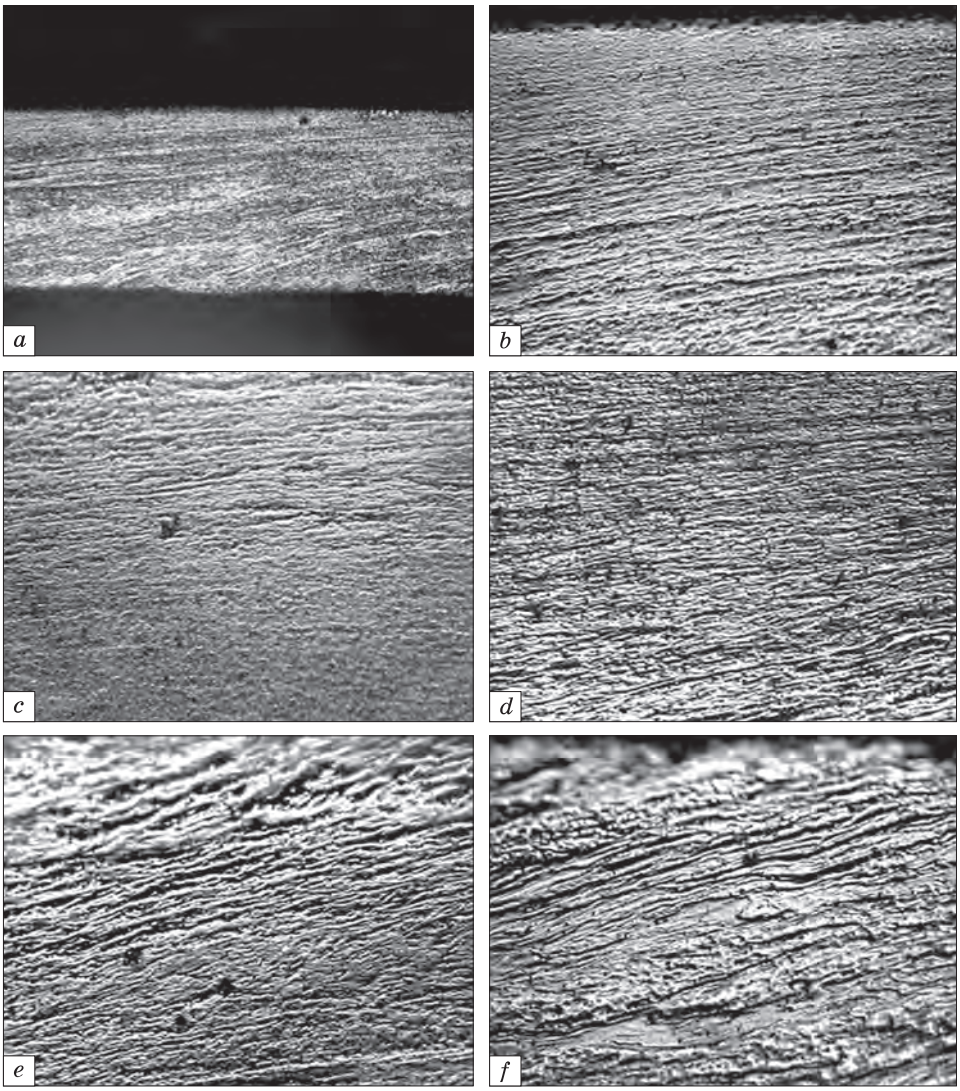

Fig. 11. The cross-section microstructures of the hot-rolled steel samples after additional deformation by THP method (N = 5, d = 9 mm) [124]: *a* — general view (×100), *b*–*f* — ×400, *e*–*f* — ×500

The regions where the active flow of the metal occurs have been observed in some areas of the sample. These are the regions with the elements of the turbulent or vortex flows and the regions of the laminar flows. Such elements and those similar to them possess the nature of the nonhomogeneous flows and are revealed at the relatively small optical magnitudes (Fig. 11, *b*) [120].

The formation of such regions evidences that the different slip systems consistently enter the process of the plastic flow; it can be fixed in

the phenomenological study of the metal deformation. According to Schmid's law [121], the slip is initiated within one or several planes, where the shear stress reaches its maximum while the rest of the planes are not active. Then, the crystal axes turn because of the shear, and a double shift, i.e., the simultaneous slip upon the two sets of planes, can occur. With the increase in the stress, the deformation begins in less favourably oriented planes. The similar turning leads to the generally crystallographic orientation of the grains, which is one of the causes of the mechanical properties anisotropy. Thus, for the plastic deformation compatibility, both the accommodation slip and accommodation turns of the lattice are necessary.

The critical moment of the partial disclination initiated in the grain boundaries can be considered as the moment of the rotational modes of plasticity occurrence in the crystal and the beginning of its fragmentation [121]. A traditional description of the plastic deformation includes the beginning of the metal plastic flow under stress; it considers only homogeneous distribution of deformation in the sample volume and takes into account only mechanical strengthening. This is a false statement, which results from the fact that theory does not take into account the main role of the temporal dependence of the gradient stress and the dissipative nature of the metal plastic flow. Considering them, one comes to the fundamentally new conclusion anticipated by the theory: without the emergence of an internal mechanical field of a vortex nature within the deformed crystal, it is impossible to have the propagation of plastic deformation through the stable crystal. The plastic flow of the metal with a stable structure is feasible only with the 'estafette' mechanism of deformation. The relaxation of one stress concentrator is to be spread throughout the sample, providing a local structural kinetic crystal transformation.

The microstructures of the sample surfaces of hot-rolled steel of 08пс grade after THP are presented in Fig. 12; these microstructures are characterized by the rotational modes presence. It means that at the stage of the developed plastic deformation, the collective effects of the evolution of the highly interacting dislocation assemblies cause rotational modes of plasticity; their carriers are partial disclinations [122]. The elements of a nonuniform flow are revealed at relatively small optical magnitudes, but they represent the upper layer of the confinement effect of the plastic deformation, that can also be clearly manifested at deeper levels. To be exact, the movement of the individual dislocation is the localization of plastic deformation, its primary spatial inhomogeneity. The plastic rotations are always accompanied by the shear. This conclusion has been proved as based on the analysis of the peculiarities of the fragmented crystal fine structure at the transition into the macro-level. Thus, the rotational instabilities not only sharply reorient the

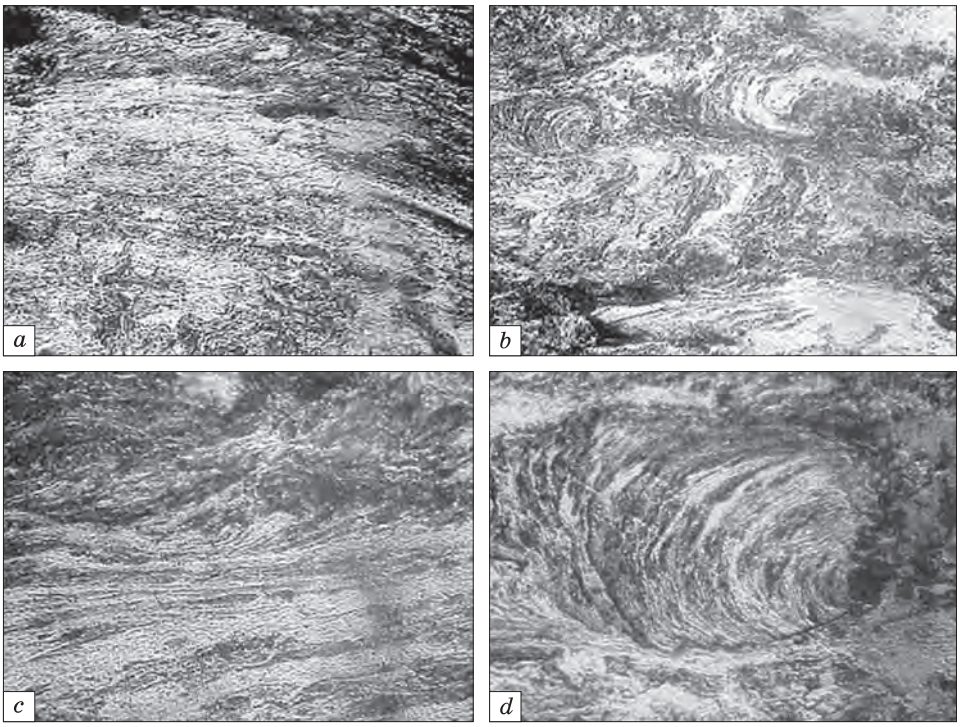

Fig. 12. The sample surface microstructures of the hot-rolled 08пс steel after additional deformation via THP, $e = 5.30$ ($N = 5$, $d = 9$ mm) [124]: *a*–*c* — ×200, *d* — ×500

crystal lattice, but also lead to the directed transfer of substances in the crystal being deformed [123]. At the late stages of the developed plastic deformation, the powerful rotation and shear instabilities occur in the fragmented structure; they are judged as the unexpected and abnormally large plastic rotations and shifts of one fragment with respect to the other one. These theory conclusions fully correlate both with the general mechanical behaviour of the material and the structural transformations under this discussion.

4.2. THP Effect on the Structure Formation of Hot-Rolled Ultra Low Carbon Steels

The world experience in the IF-steels production shows the necessity of their microalloying with niobium and titanium (in Ref. [124] these elements are introduced in the amounts of 0.02–0.04%). According to the data given in Ref. [125], the titanium content must be as much as 4.5 times carbon content. In the current studies, the titanium content in the ultralow carbon steels is higher (0.05–0.07%). The negative influence of titanium (the strengthening of material, the formation of the acute-

angled carbonitride precipitation, which make the grain boundaries brittle and reduce metal ductility) might have been compensated by the presence of 0.0002–0.0003% of calcium in the ultralow carbon steels. Calcium is a surface-active element with increased horophility to prevent the enrichment of the grain boundaries with titanium, copper and phosphorus and combines sulphur and nitrogen, as well as to improve plasticity and formability of steel [126].

The publications [127–130] presume that titanium carbides and titanium carbonitrides that precipitate from austenite block the migration of the grain boundaries; due to this, the collective and secondary ferrite recrystallization processes do not develop at steel slow cooling. In Ref. [131], the samples of the ultralow carbon steels and 08пс steel have been analysed after the deformation in two passes in the austenitic and ferrite or ferrite–pearlite temperature ranges, cooled in air and in the furnace. The ultralow carbon steel structures turned out to be similar (as the grains growth is restrained by the microparticles of titanium carbides and titanium carbonitrides), but they differed from the samples structure of 08пс steel rolled in two passes and the difference is in the size of the ferrite grains within the surface layers of the sheet. The author explains this fact by the influence of microparticles on the inhibition of the processes of the ferrite collective recrystallization. The study of the microstructure evolution in the process of imposing the load during torsion in Bridgman anvils has revealed that with the increase in the load there occurs the concentration of the dislocations in the cells, the decrease of the cell sizes and the increase of the disorientation between them. This leads to the activation of the deformation rotational modes simultaneously throughout the sample, providing a stable deformation stage [132, 133]. The elastic distortions also increase due to the distant stresses from the non-equilibrium grain boundaries containing incorporated dislocations with high densities [134–136].

The microstructure of the hot-rolled ultralow carbon steels is shown in Fig. 13. The microstructures of the 01ЮТА steel (Fig. 13, *a*, *b*) rolled in two passes (the first — in the austenite temperature range, the second — in the ferrite temperature range with 60% deformation degree and cooling in the furnace) is characterized by the presence of a fine-grained layer of 150–200 μm thickness in the surface area of the sheet. The ferrite grain size in this layer is 10–20 μm but in the central area, the grain size reaches 20–130 μm. Thus, the zonal grain-size inhomogeneity is obvious.

Further, for the microstructure of the 01ЮТ steel refer to Fig. 13, *c* and *d*. This steel has been rolled in two passes: the first — in the austenite temperature range, the second — in the ferrite temperature range with 60% deformation degree and cooling in the furnace. The microstructure is characterized by the presence of a fine-grained layer

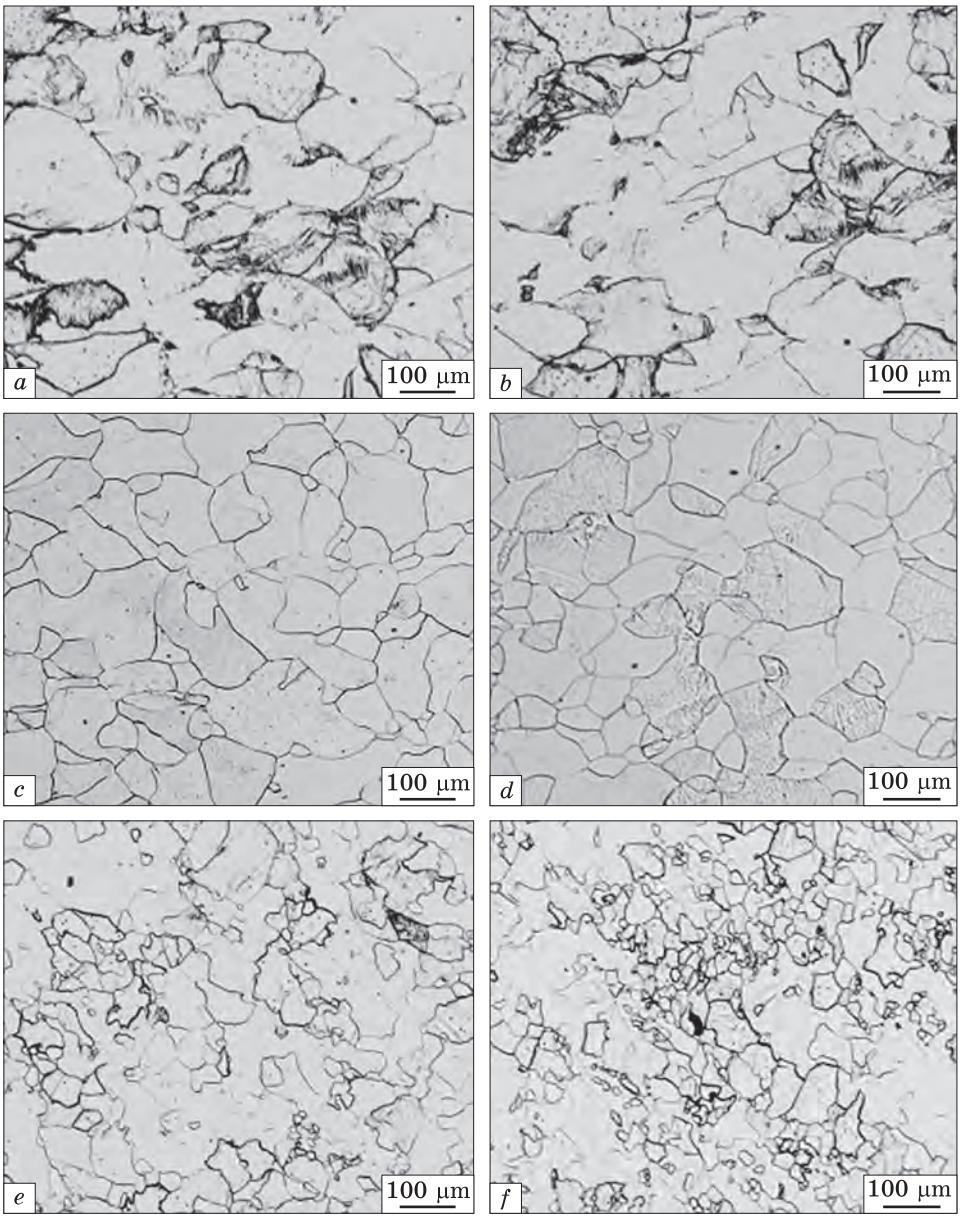

Fig. 13. The hot-rolled ultralow-carbon steel microstructures: *a* and *b* — 01Ю0ТА, *c* and *d* — 01Ю0Т, *e* and *f* — 01Ю0Т(Ca)

of 150–200 μm in thickness in some regions of the stripped steel. The ferrite grain size in the surface layer is 10–20 μm while in the central layer the size makes up 15–130 μm.

The microstructure of the 01Ю0Т(Ca) steel (Fig. 13, *e* and *f*) has been studied after the same preparation procedure as two previous

steels: 01Ю0Т(Ca) sample has been rolled in two passes: the first pass in the austenite temperature range, the second pass in the ferrite temperatures range, 60% deformation degree and cooling in the furnace. The images in Fig. 13, *e* and *f*, evidence that the microstructure is characterized by the presence of a fine-grained layer of 100–200 μm in thickness in some regions of the stripped steel. Its ferrite grain size in the surface layer is 5–20 μm while the size in the central layer of the stripped steel is 15–130 μm.

Thus, the treatment of the ultralow carbon steels (in the austenite range at the temperature of 970–980 °C, and in the ferrite range at the temperature of 730–740 °C, cooling regime in the open air ($T_{cooling}$ = = 660–680 °C)) results to the formation of the zonal grain-size inhomogeneity that may be related to the static recrystallization process. During the pause between the passes, there occurs restructuring in the ferrite. In the more rapidly cooled surface areas, a recrystallized fine-grained ferrite structure forms while the incomplete recrystallization process results in the structure as in the central area.

Authors of the publication [137] claimed that a structure with elongated ferrite grains is formed at low temperatures of the rolling completion in the surface areas of low-carbon steel sheets (at edges of the coils, which are the rapidly cooled). The slow cooling does not facilitate the completion of the recrystallization process in the central areas of the ultralow carbon steel samples.

Thus, the results of the study have shown that for obtaining a uniform structure in the ultralow carbon steel sheets treated in the last pass within the ferrite temperature interval, the decrease in $T_{cooling}$ is possible. One of the possible variants of obtaining the elongated recrystallized grains within the structure is the use of the additional heat treatment operation (the annealing is to be not higher than the temperature of A_{C1} at 690–710 °C for 3–5 hours). This will also increase the fatigue resistance of steel and improve the condition of the rolled products surface.

After hot rolling, the steels of 01Ю0ТА, 01Ю0Т and 01Ю0Т(Ca) grades were subjected to SPD by THP method. Figure 14 shows their microstructures along the radii of the samples after THP. During the torsion, the deformation scheme of a simple shear type [138–140] was embodied. This scheme is characterized by the constant change of the angle between the direction of the maximum shear stress and the direction of the maximum elongation. In the process of torsion, there occurs the new slip systems inclusion and the motion of dislocations is developing in the systems that have not been previously applied. The microstructure of the 01Ю0ТА steel is characterized by inhomogeneity of the strain distribution along the radius of the sample (Fig. 14, *a*–*c*). There are radial lines of the plastic deformation localization on the periphery of the sam-

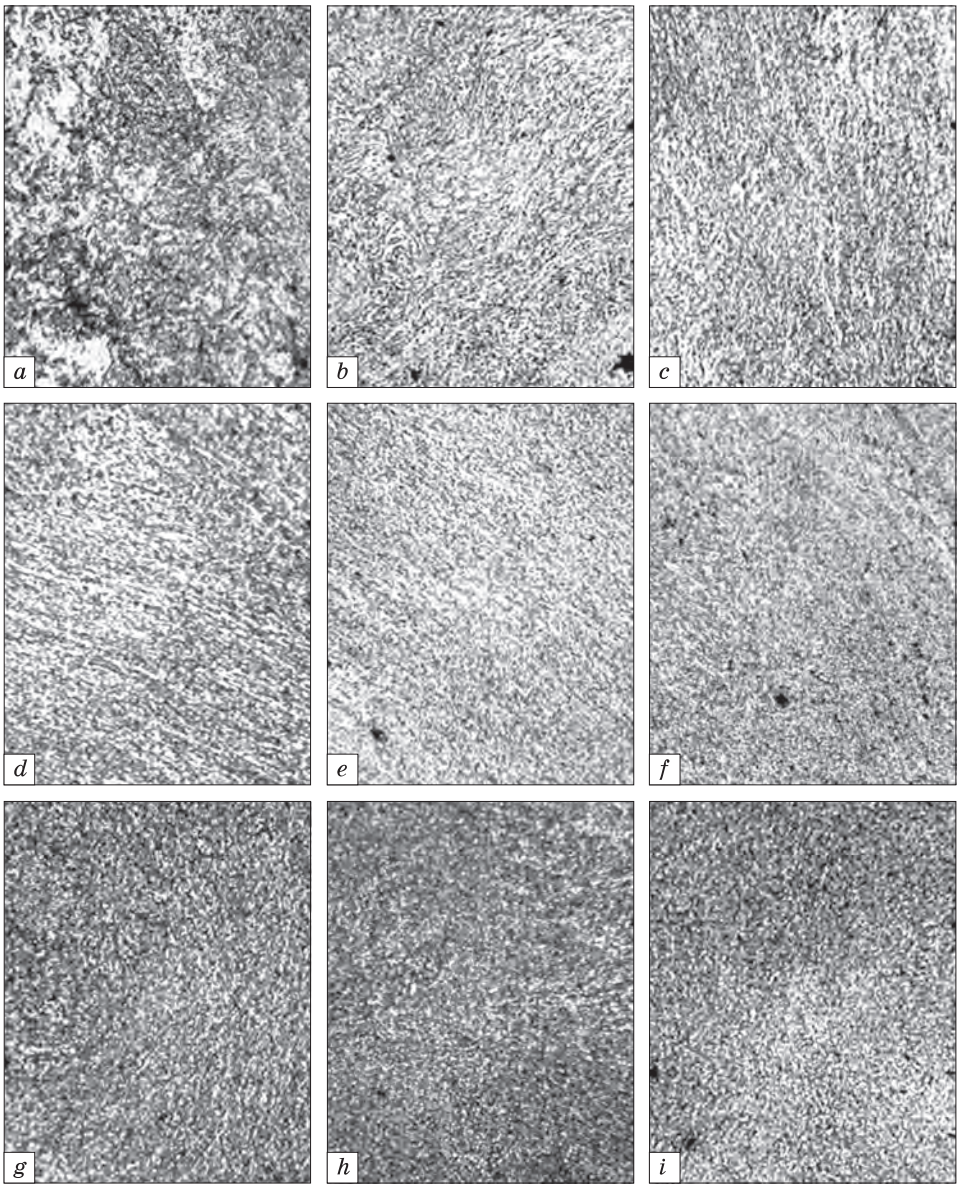

Fig. 14. The microstructure of the surface of the hot-rolled steel samples after THP: *a*, *b*, *c* — 01Ю0ТА; *d*, *e*, *f* — 01Ю0Т; *h*, *i*, *j*—01Ю0Т(Ca) (×200). Here, *a*, *d*, *g* — specimen centre; *b*, *e*, *h* — specimen middle part; *c*, *f*, *i* — specimen periphery

ple, while the sample centre has a homogeneous microstructure. The steel of 01Ю0Т grade after THP possesses a more homogeneous structure from the sample centre to the middle of its radius (Fig. 14, *d*, *e*) while on the periphery of the sample there are clearly defined strains of de-

formation that coincide with the direction of torsion (Fig. 14, *f*). At that, the grain refinement increase is also observed. Calcium in the composition of the 01ЮТ(Ca) steel affects the formation of a homogeneous structure throughout the radius of the sample (Fig. 14, *h*–*j*), that indicates about the uniform strain distribution.

5. Combined Plastic Deformation Effect on the Fine Structure and the Texture Formation of Low-Carbon and Ultralow-Carbon Steels

5.1. The Fine Structure Formation of the Low-Carbon08пс-Grade Steel after Hot Rolling

The electron-microscopic research on the thin foils of 08пс steel allows us to detect the structural changes in the course of the combined plastic deformation process. Thus, the fine structure within the surface and in the central areas of the hot-worked blank has been studied. The blank was rolled under the T_{heating} = 1000 °C, $T_{1\text{rolling}}$ = 750 °C (the two-phase austenite–ferrite temperature range), the deformation degree was 8%, the air-cooling.

Figure 15 demonstrates the electron microscopic images of the fine structure of the middle areas (Fig. 15, *a*, *b*) and the surface areas (Fig. 15, *c*, *d*) of the hot-rolled sheet steel of 08пс grade. The deformation for this steel was carried out at the temperatures of the lower range of the intercritical interval; for this reason, a significant part of austenite volume had already undergone $\gamma \rightarrow \alpha$ conversion. This can serve as an explanation why the noticeably deformed ferrite appears to be the main structural component (Fig. 15, *a*). Figure 15 shows the individual dislocations, most of them are grouped into the polygonal walls that separate the cells, and there are walls completely free of any dislocations. The size of such cells in most cases is 0.5–1.5 μm, and the maximum is 5.0 μm. In the polygonal walls, the dislocation density is small, there are individual dislocations observed, and even the regular (with hexagonal cells) fragments of the networks, which indicates active processes of diffusion at deformation temperature. Due to this fact, such dislocation networks are the low-angle ones, this fact is confirmed by the microdiffraction patterns in which the reflections are almost not split, in some cases, they show disorientation not more than 1.5–2.0° (Fig. 15, *b*).

The part of the austenite in the surface as well as in the central part of the sample of the hot-rolled sheet steel of 08пс decomposes under cooling by a diffusion mechanism to form the colonies of pearlite, which are very rarely found at the electron-microscopic analysis of thin foils (Fig. 16, *a*). Figure 16 confirms the pearlite colonies presence in the sample central area of the 08пс hot-rolled steel; this pearlite has a typi-

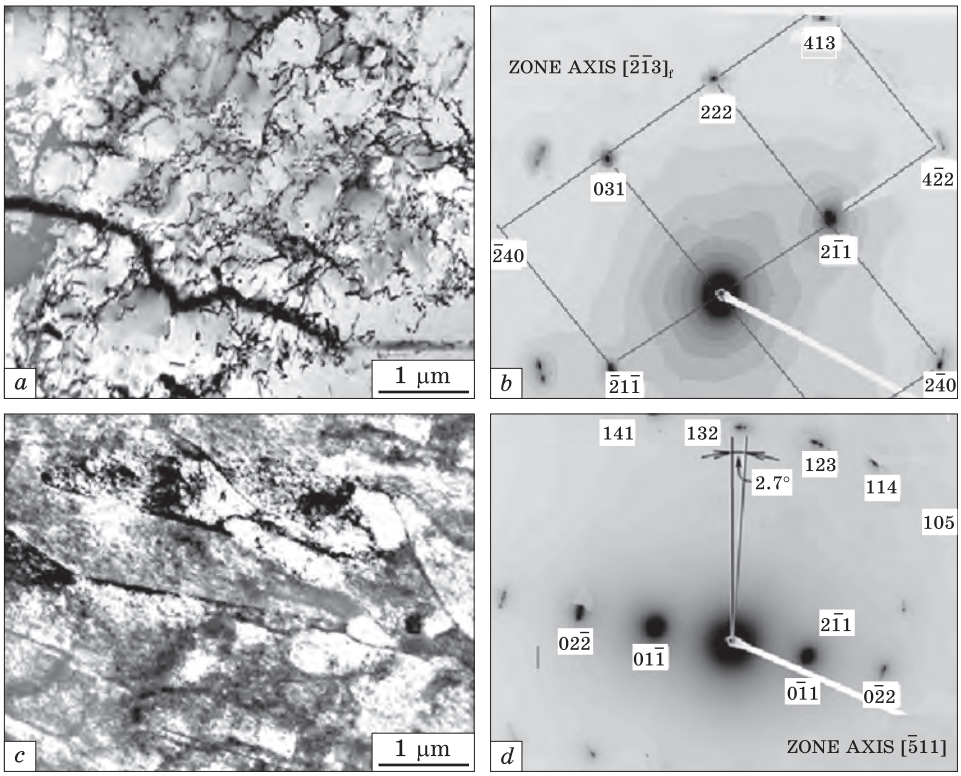

Fig. 15. The fine structure of the hot-rolled 08пс steel [155]: *a*, *b* — structure and diffraction pattern of the surface area; *c*, *d* — structure and diffraction pattern of the central area

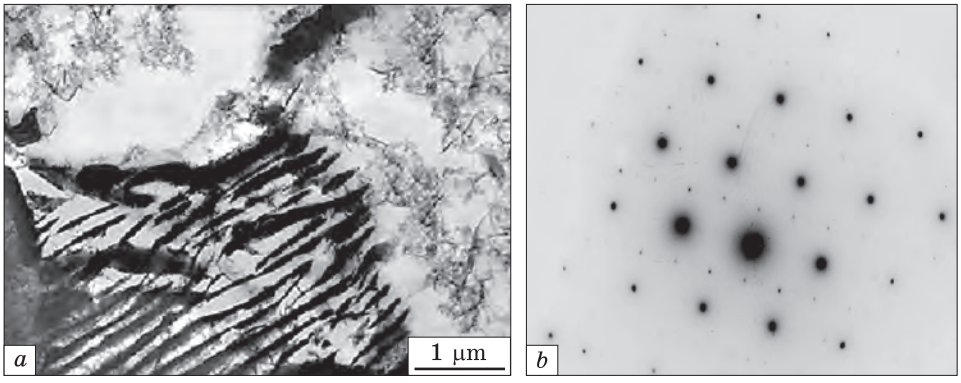

Fig. 16. The fine structure of the hot-rolled 08пс-grade steel: *a* — electron-microscopic image of the pearlite colony in the middle layer, *b* — corresponding diffraction pattern

cal laminar morphology. In general, pearlite consists of alternating plates of ferrite and cementite, and is the important structural component of carbon alloys [141]. Within the boundaries of one colony, all ferrite plates have a single 'monocrystal' orientation while, all cementite plates are of a different orientation, which is clearly confirmed by the diffraction pattern from the central part of the colony (Fig. 16, *b*).

The dispersion of the pearlite is characterized by the interlamellar spacing, i.e. defined as the sum of the thicknesses of the ferrite and the cementite plates. The interlamellar spacing reduction is accompanied by the steel strength increase. In the spheroidized state, the cementite acquires the forms of ellipsoids or spheres of different sizes, due to which such pearlite is less brittle [142]. If addressing the crystallography of the pearlite component, in this case its microdiffraction pattern demonstrates the presence of Petch-type orientation relationship between the cementite and ferrite lattice [143]. Such pearlite structure is the result of the growing in the hot-rolled austenite and it partly inherits its polygonal substructure. It should be noted that the volume per cent of the pearlite in 08пс steel is insignificant and its influence on the mechanical properties is of no consequence, however, its structural parameters can have an effect on the structural changes that occur during the subsequent intensive deformation by THP method [144]. Additionally, it is worth saying that the existence of the pearlite colonies allows the following conclusion: the process of the austenitic phase enrichment with carbon proceeds gradually and continuously from 0.08% and up to 0.8%.

5.2. Electron-Microscopic Analysis of the Fine Structure of the Hot-Rolled 08пс-Type Steel after Additional Deformation by THP

The severe plastic deformation of THP (at $N = 5$, $P = 310$ kgf/cm^2) leads to the fine-grain-structure formation if applied with the hot-rolled steel of 08пс grade (Fig. 17). Due to the ununiformed deformation distribution along the radius of the sample, it is reasonable to carry out the fine structure study on the middle of the sample radius (Fig. 17, *a*, *b*) and on its periphery (Fig. 17, *e*, *f*). The (ring) electron diffraction pattern with point reflections implies the presence of the high-angle boundaries (Fig. 17, *b*). The diffraction pattern obtained from the region located in the middle of the sample radius indicates the presence of the textured grains and their boundaries (Fig. 17, *b*). At that, the angle of the azimuthal blur is an important characteristic, which depends on the measure of the disorientation angle between the crystal lattices of individual subgrains on the image section of the sample structure. This measure is the size or the diameter of the selector diaphragm, which under given condition is 3.5 μm on the image scale. The scheme to reveal the struc-

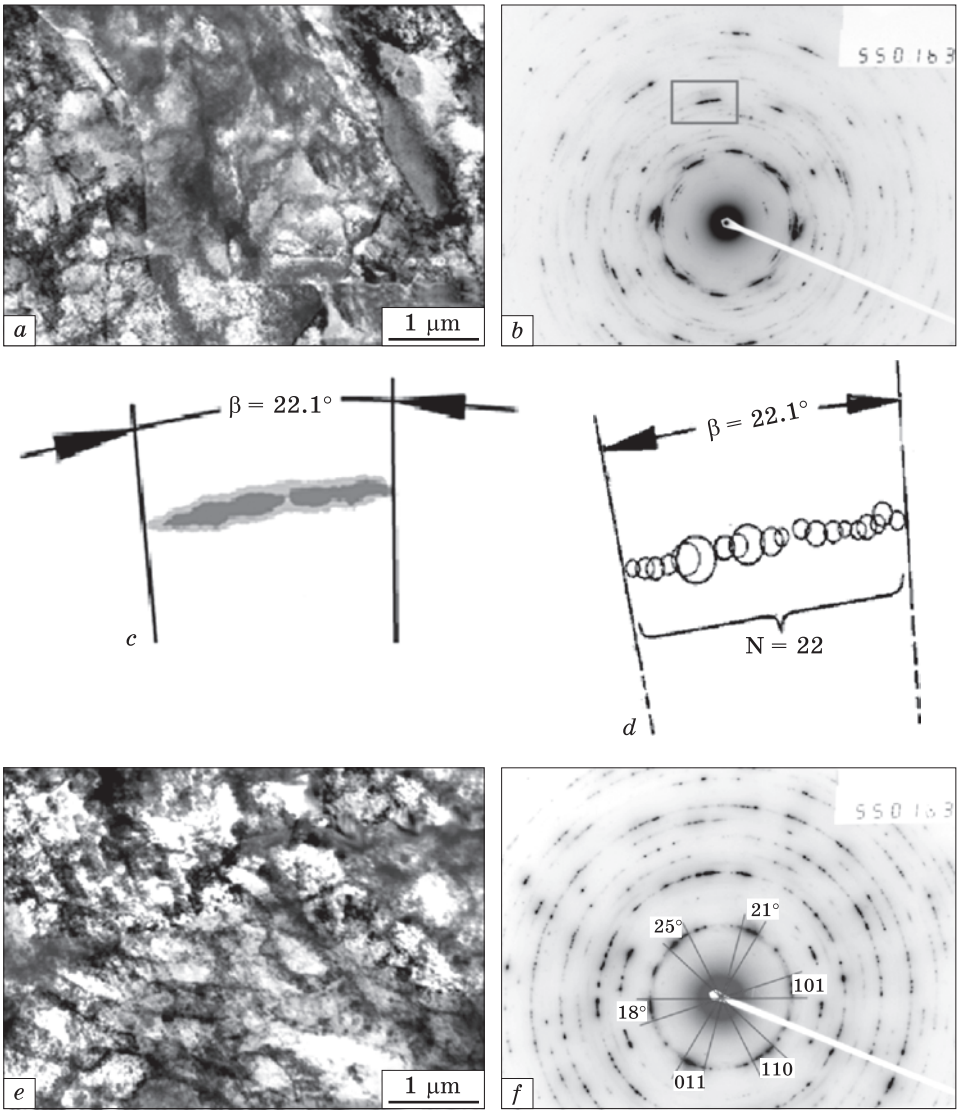

Fig. 17. The fine structure of the hot-rolled 08пс steel after additional deformation by THP method [113]: *a*, *b* — the structure and diffraction pattern of the middle of the specimen; *c*, *d* — the formation scheme for reflections; *e*, *f* — the structure and diffraction pattern of the specimen periphery

ture peculiarities of reflections that are split into subreflections is shown in Fig. 17, *c*, *d*. The region, heightened with a rectangle in Fig. 17, *b*, is shown at 8-fold magnification in Fig. 17, *c*, where via contrasting it became possible to calculate the number of the subreflexes from the polygons that form the reflection. In this case, the number of the

subgrains suitable for the diaphragm of 3.5 μm in diameter is 21 ± 3 subgrains. The azimuthal blur of the reflections in the diffraction patterns is 17–21° (Fig. 17, *d*) as related with the deformation localization on the sample periphery.

This permits bringing the conclusion that the sizes of the cells are within 0.21–1.0 μm. At that, the angles of disorientation (θ_{azim}) range from 20.5° to 26.1° (Fig. 17, *c*, *d*). On the periphery, the azimuthal blur of the reflections is rather significant, which complicates their measurement (Fig. 17, *f*). Due to this, the measurement of these angles has been carried out by the reflections of {110} type planes, which correspond to the orientation of the primary electron jet along the direction ⟨111⟩. This gives us the chance to select the angle out of 6 blurred reflections or equivalent maximums; this angle characterizes the real values of the deformation degree in the selected area. The average value has been counted by 4 microdiffraction patterns and θ_{azim} = 32.1° has been obtained.

5.3. The Fine Structure Formation of the Low-Carbon 01ЮТ(Ca)-Grade Steel after Hot Rolling

The electron-microscopic research of the thin foils from the samples of steel 01ЮТ(Ca) steel ensures the structural change tracing in the process of the tested deformation modes. The fine structure has been studied both in the surfaces and in the central areas of the worked blank and the sample rolled under the following regime: $T_{heating}$ = 1000 °C; $T_{1rolling}$ = = 970–980 °C; $T_{2rolling}$ = 730–740 °C; deformation degree: 61.5%; air-cooling. Figure 18 demonstrates the fine structure fragments of the surface area of the hot-rolled sheet steel of 01ЮТ(Ca). A similar subgrain structure of 01ЮТ steel is widespread in the hot-worked steels (Fig. 18, *a*), it appears because of the cell formation of the deformed ferrite component.

The electron-microscopic research of the sample central metal and the sample surfaces indicates the absence of the pearlite colonies within the steel, as well as the absence of the carbide precipitations both along the boundaries of the ferrite grains and in their internal volumes. The density of dislocations is somewhat increased ($\rho \approx 4.5 \cdot 10^9$ cm^{-2}) in the ferrite (Fig. 18, *a*), whereas there is an increased number of the low-angle polygonal boundaries, as a significant amount of the excess ferrite having already precipitated in the structure during the deformation in the intercritical interval (740 °C). The average cell size (the subgrains) reaches d_{sub} = 2.5 μm. One of such boundaries is located between the grains *A* and *B* in Fig. 18, *a*.

The diffraction pattern has been obtained from the region that contains the edges of the boundary (Fig. 18, *b*), due to which it looks like a

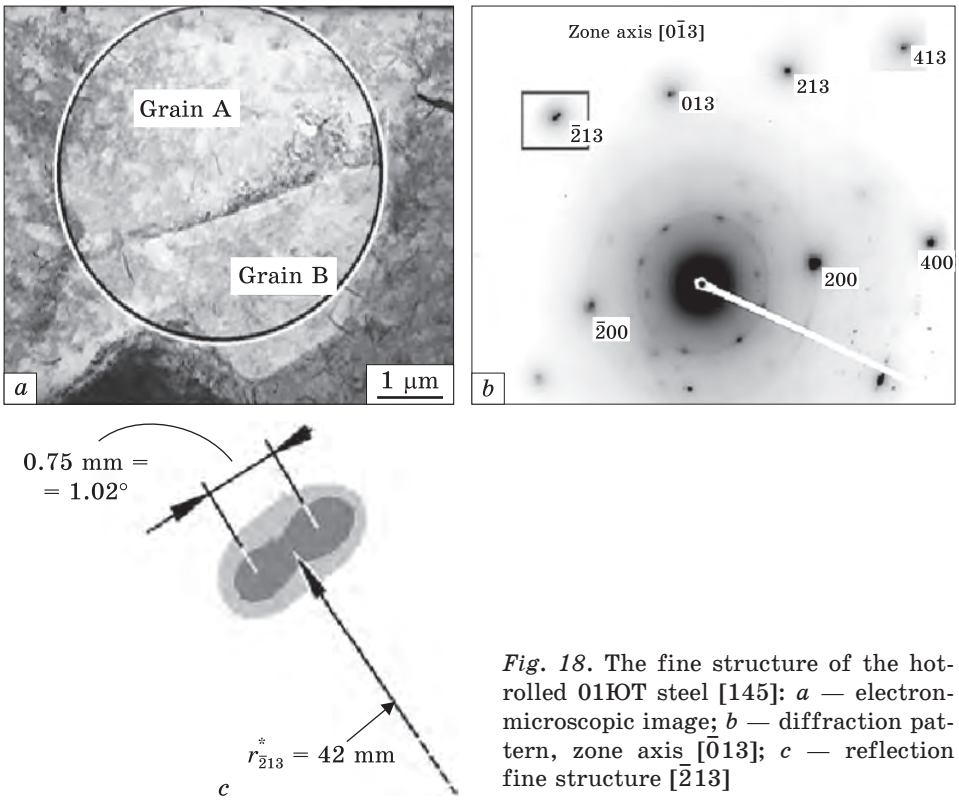

Fig. 18. The fine structure of the hot-rolled 01Ю0Т steel [145]: *a* — electron-microscopic image; *b* — diffraction pattern, zone axis [$\bar{0}$13]; *c* — reflection fine structure [$\bar{2}$13]

single-crystal one with the zone axis $[0\bar{1}3]_f$. On closer inspection of the reflections in the magnified and contrasted form (refer to Fig. 18, *c*), it becomes obvious that the boundary between the subgrains *A* and *B* has an azimuthal component of disorientation $\upsilon = 1.02°$, that corresponds to the arc distance between the reflections from the subgrains *A* and *B*. Moreover, the reflections themselves have the form of the ellipses elongated along the arc, with the radius of the reciprocal lattice $r^*_{hkl} = 42$ mm, measured on the magnified imprint of the microdiffraction pattern image (Fig. 18, *c*). This relates to the existence of the evenly distributed dislocations that are not bound into the polygonal or low-angle or subgrain boundaries, although they contribute to the higher strength of the ferrite phase.

5.4. The Electron-Microscopic Analysis of the Fine Structure of the Hot-Rolled 01Ю0Т(Ca)-Type Steel after Additional Deformation by THP

The electron-microscopic research on the thin foils of the hot-rolled ultralow-carbon steel of 01Ю0Т(Ca) grade allows detecting the structural changes in the process of SPD by THP method ($N = 5$, $P = 310$ kgf/cm^2).

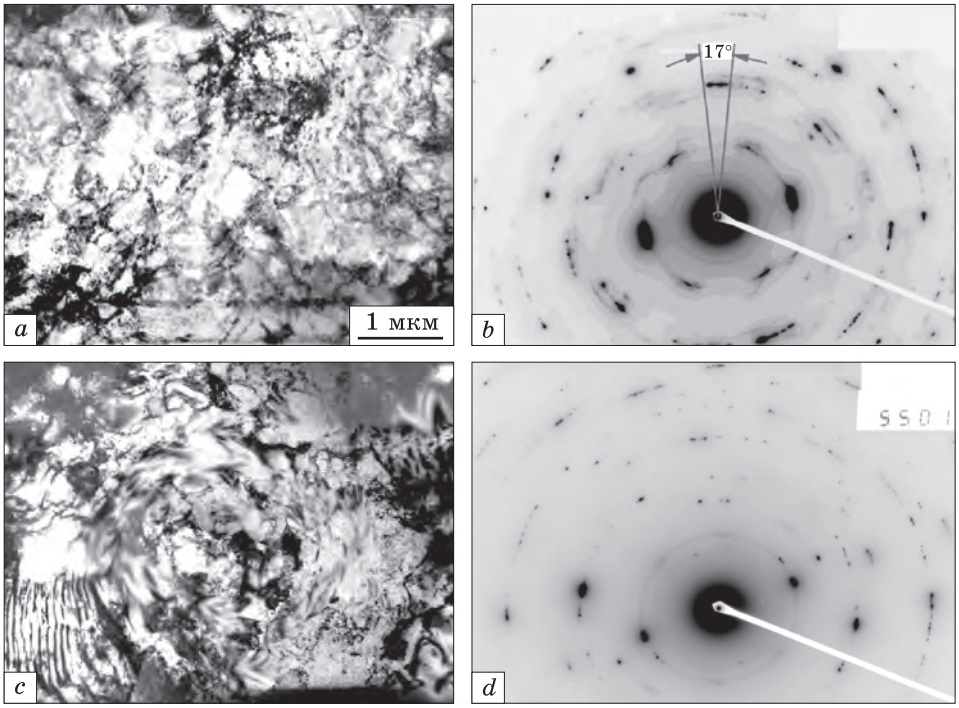

Fig. 19. The fine structure of the hot-rolled 01Ю0Т(Ca)-type steel after additional deformation by THP [145], where *a* and *b* — structure and diffraction pattern of the middle of the sample, *c* and *d* — structure and diffraction pattern of the sample periphery

The fine structure of the radius middle part of the disk sample made from the hot-rolled ultralow-carbon steel of 01Ю0Т(Ca) after additional deformation by THP method is given in Fig. 19, *a*.

The deformation after hot rolling is distributed directly along the radius of the disk sample, and this inhomogeneity is evident in the dislocation cell structure both in the fine structure images and in the microdiffraction patterns. The effect of deformation is visible in the change of the cell sizes, which are characterized by the presence of the azimuthally blurred diffraction reflections of the microdiffraction patterns (Fig. 19, *b*). Due to the deformation localization at the periphery of the sample, the azimuthal blurring of the reflections is 17–21° in the diffraction patterns (Fig. 19, *d*). In this case, it should be noted that the image of the main reflection splitting has a centrosymmetric nature that is characteristic of the vortex flow of the metal when there are micro regions of rotation accompanied by the emergence of the rotational modes. The size of the microcells with such rotational character is 2–5 μm in diameter and more. Thus, it can be assumed, that in the central part of such cyclonic formations the density of dislocations is somewhat lower than on the periphery (Fig. 19, *c*).

5.5. The Study on the Texture of Low-Carbon Hot-Rolled 08пс Steel after THP via EBSD Analysis

The preferential orientation of the texture has a significant effect on the structure-dependent properties of the polycrystalline substance. The survey of the publications [146, 147] devoted to the study of the texture formation processes and the mechanisms of the polycrystals deformation with the b.c.c. arrangement has revealed that the systematic study of the textures has not been carried out, though these data are of scientific and practical interest. EBSD method probes different crystal planes with the electrons. In these types of studies, there are especially high requirements for the quality of the surface; due to this, the samples have been subjected to the electrolytic polishing in order to obtain mirror-like surfaces at high speed with the absence of the field distortion in the surface layer. It is important to have a detailed description of the deformation methods, since not only the sample microstructure but also the methods of its surface preparation for the EBSD research depend on the history of the sample processing. It is known that during the preparation of the polished sections, the non-deformed material and the deformed material behave differently. The results of the EBSD studies depend on the quality of the structure preparation. A quality structure with minimal distortion is obtained when using non-deformed material while the deformed material requires more careful preparation at the polishing stage.

The surface of each sample has been previously studied with an optical microscope in order to select the areas for the research among the sample surface and its central zones. However, with the development of the SPD methods, a number of specific problems arise related to the identification of dynamically recrystallized grains formed during the deformation process. The textured material can be considered as an intermediate state between a material with a chaotic distribution of its orientations and the material with the ideal orientations. One of the features of the texture is scattering, that is the deviation of the grain orientations from a certain medium. One of the ways to define a texture is to describe its ideal orientation of the single crystals with observance for their scattering phenomenon. Based on EBSD analysis for the orientation scanning, the orientation distribution functions are constructed at each point of its direction.

The data on the texture type and its scattering have been obtained after determining the orientation of each grain individually. For the known orientation of a larger number of grains, the direct pole figures have been constructed for planes {100}, {110}, {111}. Aiming at the texture description, the direct pole figure and inverse pole figures are applied. Every pole figure is the average value of the grain distribution

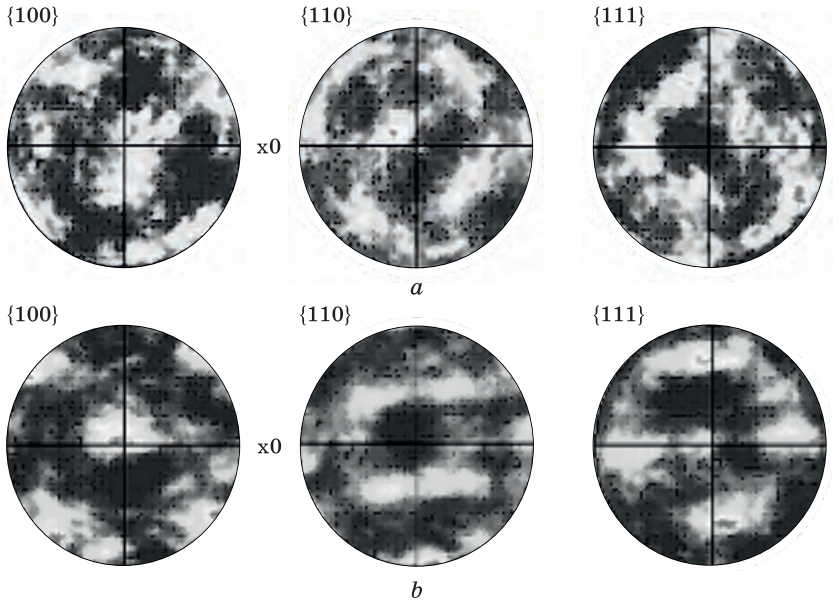

Fig. 20. Quantitative direct pole figures intensity within the texture of the hot-rolled 08пс steel after hydrostatic pressure processing: *a* — sample central part, while *b* — sample periphery

over the spatial orientations. The texture of polycrystals can be described via four coordinates. Three of them determine the grain orientations while the fourth defines its density (its possible orientation). Therefore, even the presence of several pole figures does not enable the establishing the quantitative connection between the properties of the material and its texture. The direct pole figures of the hot-rolled low-carbon steel of 08пс after additional deformation by means of hydrostatic pressure are shown in Fig. 20.

If we assume that in the hot-rolling process, the friction stress in the deformation zone causes the formation of certain shear bands on the metal surface, and these shear bands possess the different crystallographic parameters than the internal metal [148] and the recrystallization processes are different within them as well. The development of recrystallization in the mentioned metal with, so-called Goss texture [149], (110) (001), is characterized by faster rates of nuclei formation than those within the metal with other texture parameters. The high rate of growth in the ferrite grains in this case is conditioned by recrystallization mechanism grounded on grain coalescence.

The components from the hot-rolled steel of 08пс grade acquire certain texture characteristic features after processing additionally with THP methods and these characteristics are: (100), (110), (111). In the central zone of the sample, the Goss texture is obviously singled out and

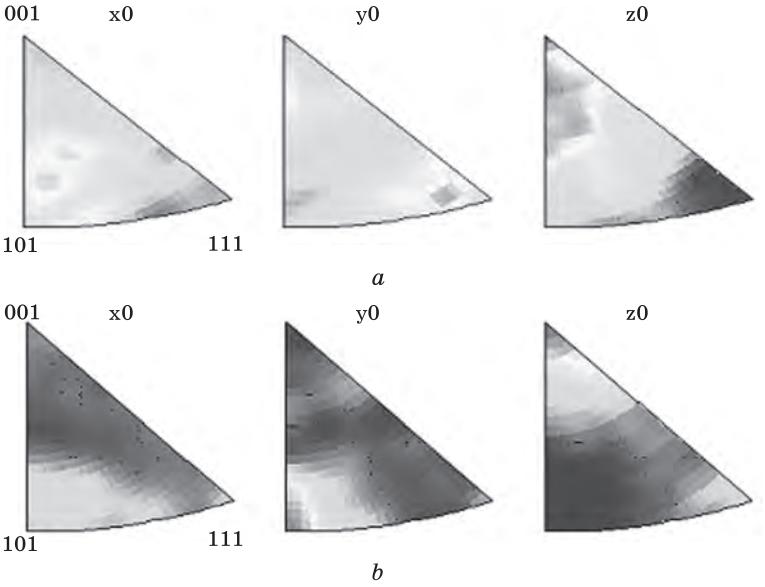

Fig. 21. Inverse pole figures of hot-rolled 08пс steel subjected to the further SPD by the THP methods: *a* — sample central part, *b* — sample periphery

it is the feature of the hot-rolled state that is confirmed by inheriting the texture of hot-rolled metal with further cold SPD by THP method.

The publication [150] notes that the lattices of the majority of Fe_α crystals are arranged in a way to have the crystallographic directions of sliding ⟨111⟩ within the plane parallel to the rolling plane. This enhances the elongation properties of the cold-rolled sheet. The shape of the recrystallized ferrite grains facilitate this: they are elongated along the rolling direction, that is, the ratio of the two axes of the grain is more than 1. The analysis carried out for inverse pole figures evidences that there is the presence of the texture components of (101) and (001), they have their maximal intensity in the sample periphery in the directions of 0*Y* and 0*Z* (Fig. 21, *b*).

5.6. The EBSD Analysis of the Texture of the Hot-Rolled Ultralow-Carbon 01Ю0Т(Ca)-Grade Steel after THP

The texture characteristic (intensity, scattering, orientation ratio) change before the sheet intersection. It is due to the deformation inhomogeneity via the influence of the friction forces acting from the rolling roll on the surfaces in contact. Therefore, the velocity of the metal flow in the internal metal is higher than that on the surface. The resulting texture of the central metal is more precisely expressed. Moreover, the surface layers are often characterized by new orientations, which are

not typical for the deformation texture and their presence depends on the deformation scheme, temperature and degree. If due to the sudden temperature drop, the texture of recrystallization is formed along with preserving the deformation texture within the internal metal, then the inhomogeneity of the texture is more visible. For the material with b.c.c. lattice, the transition to the surface layers shows the lower intensity and greater scattering of the texture. The less is the deformation degree and the thicker is the sample, the better the texture inhomogeneity is expressed in it.

The pole figures allow us to judge on the texture intensity and its scattering. In order to compare to examples of direct pole figures with different degrees of lattice distortions (different deformation degree and processing regimes), let us construct the levels of pole density. The intensity, which is averaged per the whole pole figure, is taken as a unit of pole density level to correspond to the chaotic orientation of the crystals [151].

One of the texture characteristics is its intensity that is the density unit filling the dedicated orientation of the {*hkl*} lattice by planes. The pole figures establish the ratios between the crystallographic elements and the conventional external directions of the sample. The colour contours on the direct pole figures indicate the intensity of the texture as compared with the chaotic texture. The yellow and the orange colours identify the minimal and the maximal values of the pole density in the units divisible by the chaotic distribution. The points with close values of intensity are connected with isolines. The pole figures of hot-cold 01Ю0Т(Ca) steel for the planes of (100), (110), and (111) are shown in Fig. 22.

Though for b.c.c. metals it is sufficient to demonstrate the changes in the pole figures (110), we present the figures for three most significant directions of the cubic crystal. The best expressed in the sample central zone of 01Ю0Т(Ca) steel is the texture with the dominating orientation of the ferrite grains biplane {100} (Fig. 22, *a*). The structure inhomogeneity is observed in the intersection of the sheet rolled in two passes: in the central zone there is the best texture of {100} type while for the surface zone there are texture structures unity of {100} and {111}. The texture of the sample central zone is characterized by higher intensity than the texture of fine grains: the orientation pole density of ⟨100⟩ decreases if compared with surface layer with $P_{\langle 100\rangle} = 6.2$ until $P_{\langle 100\rangle} = 4.3$ (Fig. 22).

Thus, according to the data submitted in Ref. [152], the velocity of metal flow in the internal metal is higher than that in the surface layer due to the inhomogeneity of the deformation. As the result, the texture in the central metal is better expressed. Therefore, through the whole cross-section of the sample processed in the regime, the ordinary textures of rolling formed with better expressed orientation are {100} and {111}.

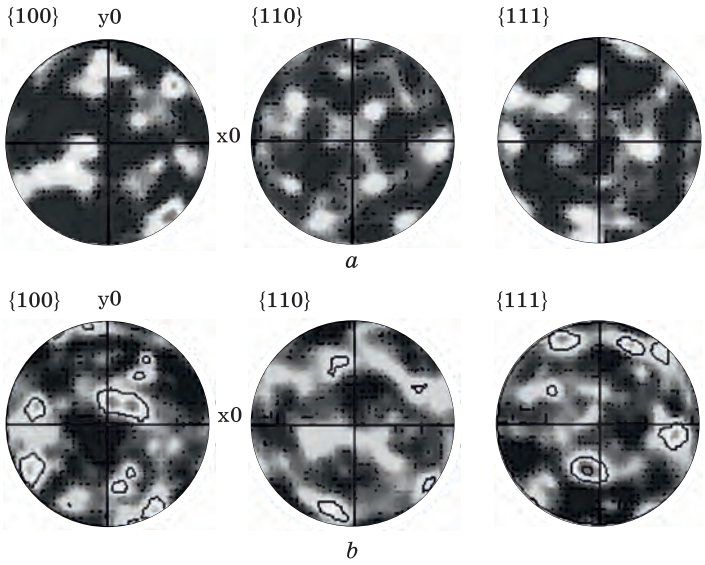

Fig. 22. Quantitative intensity of direct pole figures within the hot-rolled steel texture of 01ЮТ(Ca)-type: *a* — sample central part, *b* — sample periphery

As known from Refs. [153–158], the favourable is that texture wherein the large part of the grain lattices is orientated in a way to arrange their crystallographic plane {111} parallel to the sheet surface. The technology of IF-steel has to provide the preparation of the maximal amounts of the grains with such orientation.

The plastic effect within the metal occurs on condition that the resistance to the shear is higher than the ultimate one in some of the lattice zones. In this case, sliding occurs on the plane towards the closest packed atoms. For ferrite, this direction is the cube diagonal (111). Within the ferrite grains, the lines of sliding are rarely straight lines, unlike those of austenite. The ferrite grains are covered with bent-up lines that are arranged on one or several middle directions. If the new system of sliding lines intersects the previously formed lines, then the value of sliding can be determined through the shears of those lines, which have appeared earlier.

In Ref. [159], the differences in the textures of the surface and the central zone of IF-samples are explained by decarburization of the sample surfaces under metallic scales.

Figure 23 demonstrates the direct pole figures of 01ЮТ(Ca) steel after THP processing at room temperature. The noticeable increase of the intensity peaks is found and this leads to formation of the less blur structure within the central zone of the sample (Fig. 23, *a*) as compared with the central zone of the initial state (Fig. 23, *a*).

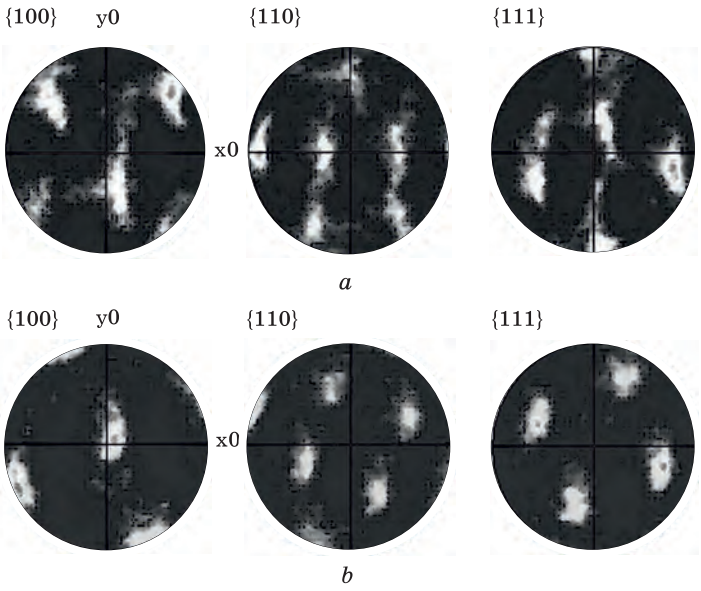

Fig. 23. Quantitative intensity of direct pole figures within the texture of the hot-rolled 01Ю0Т(Ca) steel after additional deformation by THP methods: *a* — sample central part, *b* — sample periphery

The analysis of direct pole figures of 01Ю0Т(Ca) steel after THP processing has shown that the deformation at torsion leads to the higher intensity values in the sample periphery and therefore to forming more precisely distinguished texture. The specific feature of the texture after additional cold deformation by THP method is the inheriting the rolling texture with the components of {100} and {111}. After THP, the new component of {110} changes the texture.

The interpretation of the data obtained for the textures is the given in Refs. [160, 161]. The action of the crystallographically observed mechanisms of deformation, including sliding and twinning at certain crystallographic planes and directions, leads to the development of the crystallographic texture within the metal being deformed. While the deformation due to the mutual shear of grains is developed at non-crystallographic intergrain boundaries, it is not related to the formation of crystallographic texture and causes texture weakening and scatting in the initial metal.

From the above considerations, it is easily deduced that crystallographic sliding leads to the sample texture enhancing while the non- crystallographic mechanisms of plastic deformation cause the blurred texture.

Thus, in the process of deformation the following mechanism of grain shears has been actively developed. Moreover, the influence of the

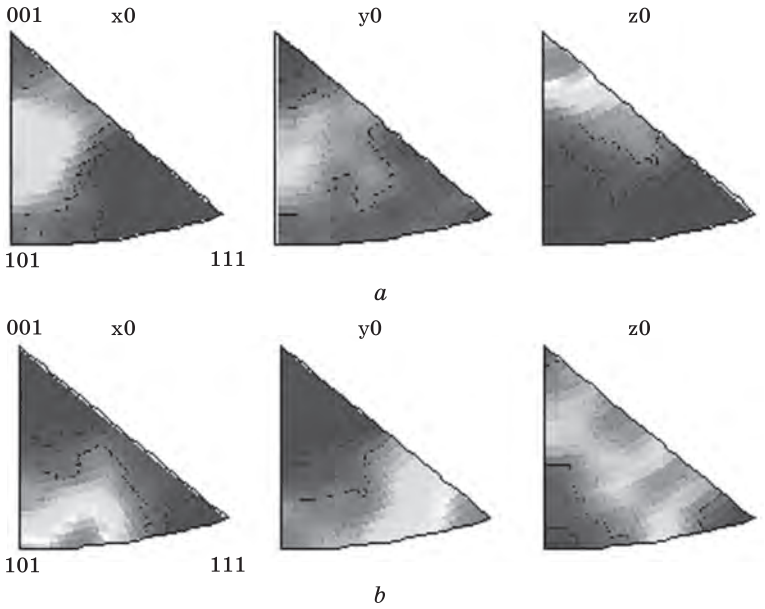

Fig. 24. Inverse pole figures of hot-rolled 01Ю0Т(Ca) steel followed with further SPD by THP method: *a* — sample central part, *b* — sample periphery

crystallographic sliding cannot be neglected, though its contribution to the texture formation is less expressed.

The maps of the inverse poles are united into the organization chart with the crystallographic description of the single direction of reference. These maps indicate the principle directions within the sample and the intersections of the directions. At each point of the map, the crystallographic direction corresponds to the certain direction in the sample, and the colour is distributed in accordance to its position in b.c.c. lattice. The orientations of certain crystallographic directions are encoded in the dedicated colours on the crystal orientation maps. The analysis on the inverse pole figures provides information not only about the presence of a texture within the sample, but also about the mechanisms occurring during the processing. Thus, as an example can serve the case when the predominance of one of the pole densities can indicate which relief mechanism specifically prevails in the given sample: interstitial or intergranular slip while the changes in the texture can be related to the changes in the deformation mechanisms or the development of dynamic recrystallization [162]. Moreover, if the maximum pole density is concentrated in the orientation range of ⟨111⟩ and ⟨110⟩, then this evidences that the mechanisms of twinning have been actively developed in the sample [163]. If the intensity of the normal yield decreases and the distribution becomes more homogeneous, which is observed in our case, and then we can speak about the texture blurring

and the activation of non-crystallographic mechanisms of plastic deformation.

However, the texture analysis will not be complete without the analysis of direct pole figures. They show the density of the normal yield of the corresponding crystallographic planes, in this case they are ⟨111⟩, ⟨110⟩, ⟨100⟩. Consider the effect of THP on the formation of a texture in terms of inverse pole figures. In Figure 24, we demonstrate the inverse pole figures in the crystal of the steel 01Ю0ТТ (Ca) after they have been subjected to THP into different external directions: the direction of deformation (0*X*), the transverse direction (0*Y*), the normal direction (0*Z*) (direction of inverse pole figures) for cubic crystals ⟨100⟩, ⟨110⟩, and ⟨111⟩.

In the central zone of the sample (Fig. 24, *a*), the maximum density is concentrated in the direction of ⟨001⟩ (inverse pole figures). The maximum pole density is observed in the direction of ⟨101⟩ and is concentrated near the direction of ⟨111⟩ (Fig. 24, *b*). In other directions (transverse and axial), the principle changes have not been registered. Further, the inverse pole figures becoming more acute indicate the presence of crystallographic deformation mechanisms during the processing procedure, for example, internal grain slip (Fig. 24, *b*).

6. Nanoindentation Method for Defining Strength and Ductility of Hot-Rolled 08пс-, 01Ю0ТА-, 01Ю0Т-, and 01Ю0Т(СА)-Grade Steels after Their Additional Cold Deformation

6.1. Strength Characteristics Determination by S.O. Firstov Methodology Applied for Hot-Rolled 08пс, 01Ю0ТА, 01Ю0Т, and 01Ю0Т(Ca) Steels after Their THP Processing

Nanoindentation is currently reported to be the principle method for determining the physical and mechanical characteristics of various materials and coatings according to the nanoscale. Via this method, different mechanical characteristics of the material can be reported in a number up to 20 [164, 165].

Aiming at determining how the method of nanoindentation reveals the metallic material mechanical properties, international standards (e.g. ISO 14577) have been developed and adopted. Moreover, a few factors significantly affect the results of whatever mechanical tests conducted by this method. They are surface roughness, temperature drift, imperfect indenter geometry, peculiarities of the material structure and others. Further, there are the methods developed for data processing and sample preparation, which take into account thereof factors [166, 167].

The property of hardness is an issue of special concern among the methods of material quality control. Thereof is the fastest, simplest and non-destructive method of analysis. Moreover, there exist methods addressing to the other mechanical properties that have a correlation with the hardness [168]. Further, the hardness measurements are used to test the quality of sheet steel. These properties do not bring the conclusions concerning the behaviour of steel during pressing, but very often, the sheets with a low hardness are well pressed [169]. The publications [170, 171] utilize the assumptions [172] for the first purpose of elaborating the detailed method for the Young's modulus determining and for the second purpose of obtaining reliable values of hardness. The particular attention is drawn to the fact that the indenter penetration depth registered in the indentation diagram does not coincide with the depth of its imprint during which the contact between the indenter and the material takes place. In this connection [173, 174], the value of the *hc* penetration depth is introduced, wherein the contact between the indenter and the material occurs after the complete load until $P_{\max}$. In this part of the indentation imprint, there occurs an elastic-plastic deformation and possible destruction of the material, as well as the elastic deformation of the indenter.

In Ref. [175], the possible physical causes of the scale effect within the materials are considered during testing by nanoindentation. Thus, the experiments on nanoindentation enable the further studies on the relation between the structure and the mechanical properties of a wide range of materials at the nanoscale. These studies are important when designing materials with a given set of properties.

6.1.1. Indentation Hardness Calculation

The indentation hardness with the applied force ($P_{\max}$) in the contact area of the indentation imprint (h_c) can be expressed as follows:

$$H_{IT} = \frac{P_{\max}}{24.5\, h_c^2}, \tag{6.1}$$

where $P_{\max}$ is an applied force (N), h_c is a penetration depth formed by the contact between the indenter and the material after the complete load (until $P_{\max}$).

$$h_c = h_{\max} - 0.75 \frac{p_{\max}}{dp/dh_{\max}}. \tag{6.2}$$

The indentation hardness with utilization of the work (W_c) performed by the applied force ($F_{\max}$) for the displacement of the material by the indenter within the contact area of the indentation imprint can be defined as follows:

$$H_{Wc} = 0.843\, H_{IT}, \tag{6.3}$$

where H_{IT} is indentation hardness (GPa).

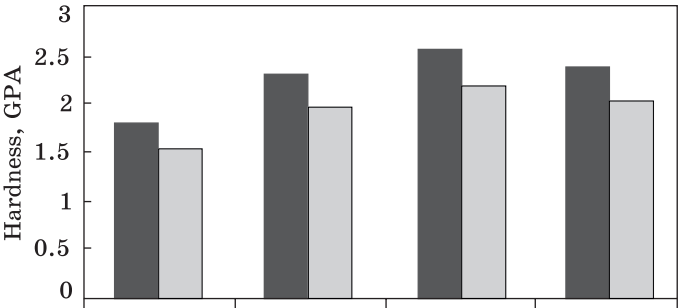

	Initial state	1	2	3
H_{IT}	1.823	2.3222	2.558	2.382
H_{we}	1.548	1.957	2.156	2.007

a

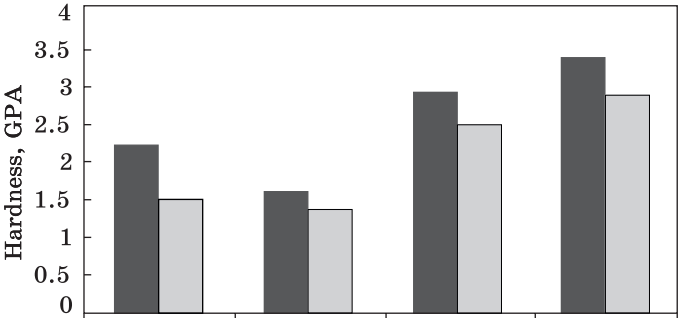

	Initial state	1	2	3
H_{IT}	2.235	1.621	2.938	3.409
H_{we}	1.554	1.366	2.477	2.873

b

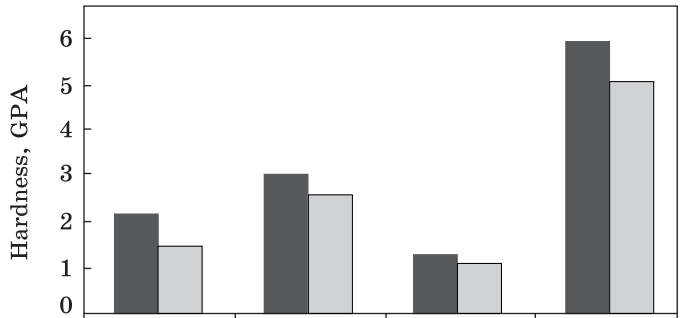

	Initial state	1	2	3
H_{IT}	2.213	2.965	1.299	5.879
H_{we}	1.444	2.495	1.0942	4.956

c

Fig. 25. Distribution of the indentation hardness along the sample radius for ultralow-carbon steel sample in the initial hot-rolled state and in the state after additional strain by the THP method. Here, *1* — sample centre, *2* — sample middle radius, *3* — sample periphery; *a*—01ЮТА (N = 5), *b* — 01ЮТ (N = 5), *c* — 01ЮТ(Ca) (N = 3)

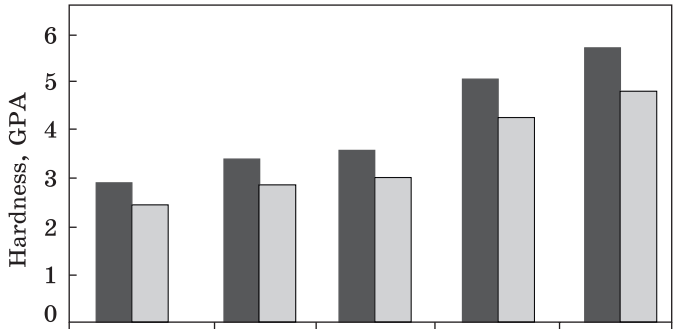

	Initial state	1	2	3	4
H_{IT}	2.921	3.423	3.584	5.1	5.737
H_{We}	2.462	2.866	3.021	4.2993	4.83

Fig. 26. Distribution of the indentation hardness along the sample radius of 08пс steel in the initial hot-rolled state and that after the additional strain by the THP method (N = 5): *1* — sample centre, *2* — middle of sample radius; *3*, *4* — sample periphery

Figure 25 illustrates the distribution of the indentation hardness and the hardness of the work along the sample radius after the THP operations with the 01Ю0ТА, 01Ю0Т, and 01Ю0Т(Ca) steels. It has been established that after THP processing, the steels of 01Ю0ТА and 01Ю0Т show the same type of the hardness change along the radius of the sample. From the sample centre to the sample middle metal, the hardness increases in both steels: 2.1 and 2.6 GPa in 01Ю0ТА while 2.5 and 2.9 GPa in the 01Ю0Т. At the periphery there is a decrease observed in the hardness of 01Ю0ТА steel down to 2.0 and 2.3 GPa. The changes in the hardness of 01Ю0Т(Ca) and 01Ю0Т at THP are different in their nature: the maximum hardness values are observed at the periphery of the sample and reach 4.9 and 5.8 GPa 01Ю0Т(Ca), and those for 01Ю0Т are 2.9 and 3.4 GPa.

For all the cases studied with the ultralow-carbon steel, the hardness increase has been found during the THP processing both in the centre and at the periphery of the sample. The nonhomogeneous distribution of the hardness along the sample radius of the sample is explained as the result of the deformation localization at the periphery of the sample.

In Figure 26, we demonstrate how are distributed the indentation hardness and the hardness obtained via the work along the 08пс sample radius after THP processing. The attained results allow us to claim that the hardness of the 08пс steel after THP processing varies over the radius of the sample: from its centre to its periphery, the hardness increases: H_1 = 3.4 GPa and H_4 = 6.0 GPa, respectively.

The hardness values calculated per the work parameter are slightly lower than the indentation hardness and vary from 2.9 to 4.8 GPa. The value of the hardness on the sample periphery is 2 times higher than the hardness of this steel in the initial hot-rolled state. This also confirms the fact of the deformation localization on the periphery of the sample [176].

6.1.2. Calculation of Noncontact Elastic Strain and Corresponding Stresses in the Hot-Rolled Low-Carbon and Ultralow-Carbon Steels Subjected to Additional Deformation via THP Methods

The Ref. [177] reports on the correlation revealed that determines the elastic deformation of not completely recovered nature in the material indentation imprint (when the elastic deformation is only a part of the elastic-plastic deformation). It is able to describe only that part of the elastic deformation which is manifested in the non-contact region of the indentation imprint, that is, it is related to the material located within the deepening around the indenter (the material 'feels' elastic deformation, ε_{es}, only). In order to calculate the non-contact elastic deformation during the indentation the following formula is applied [176]:

$$\varepsilon_{es} = 0.0984 \times (h_s/h_c) = 0.307 \times (H_{IT}/E^*), \qquad (6.4)$$

where h_s is the indenter penetration depth (no contact with the material resulting in the material deepening around the indenter), h_c is the indenter penetration depth (contact between the material and the indenter after complete load until P_{max}), H_{IT}/E^* is the material resistant to the applied stress.

The non-contact elastic deformation of hot-rolled ultralow-carbon steels after additional plastic deformation by torsion under hydrostatic pressure has been calculated according to formula (6.4) and the results are presented in Fig. 27.

The method of automatic indentation allows defining the limit value of the elastic deformation, which can be reached within the material: $\varepsilon_{es}^{limit} = 0.5626 \ln(\sin\alpha)$ ($\varepsilon_{es}^{limit} \approx 5.5\%$ for a standard Berkovich indenter). Depending on the material and the conditions of its loading, this value may be sufficient or insufficient to complete its real elastic properties. The calculated values of the elastic deformation occurring along the sample radius of ultra-low carbon steels are presented in Fig. 27.

The analysis on the image in Fig. 27 confirms the fact of the uniform distribution of deformation along the radius of the ultralow-carbon steel sample. In the initial hot-rolled state, the values of ε_{es} are as follows: for 01Ю0ТА steel, $\varepsilon_{es} = 0.00287$; for 01Ю0Т steel, $\varepsilon_{es} = 0.00423$, while for 01Ю0Т(Ca) steel, $\varepsilon_{es} = 0.0033$. In the process of THP processing, the value of ε_{es} increases from the sample centre to its periphery as

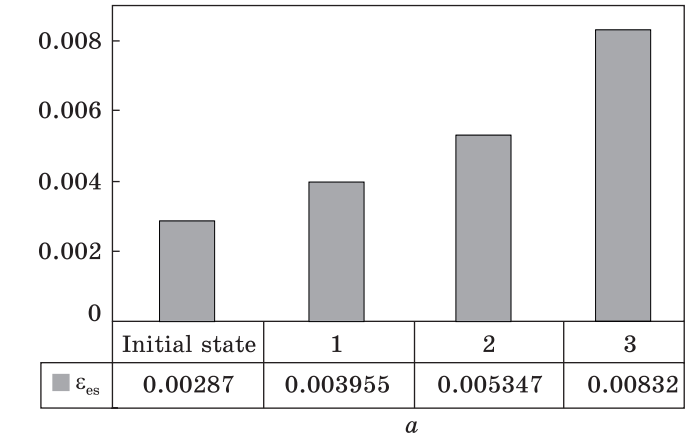

a

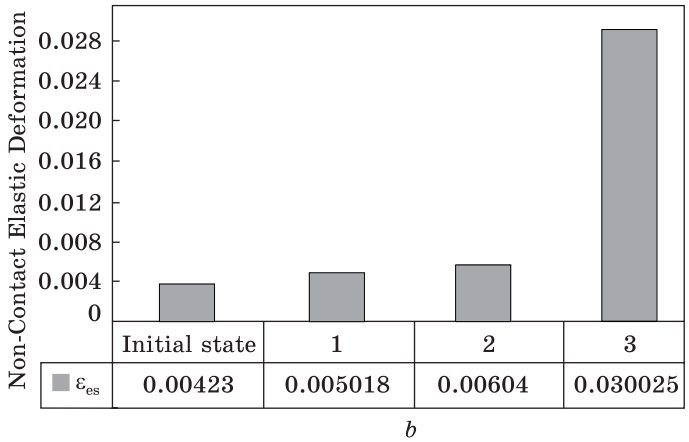

b

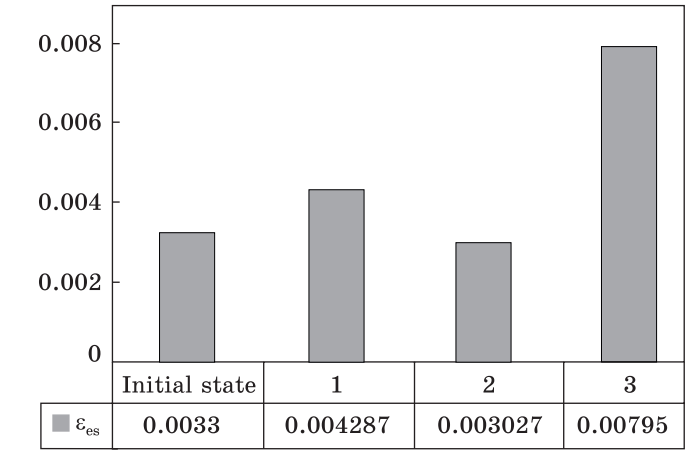

c

Fig. 27. Distribution of the calculated values of elastic deformation along the sample radius of the hot-rolled ultralow-carbon steel (in the initial hot-rolled state and after additional strain by the THP methods): *1* — sample centre, *2* — middle of sample radius, *3* — sample periphery; *a* — 01Ю0ТА, *b* — 01Ю0Т, *c* — 01Ю0Т(Ca)

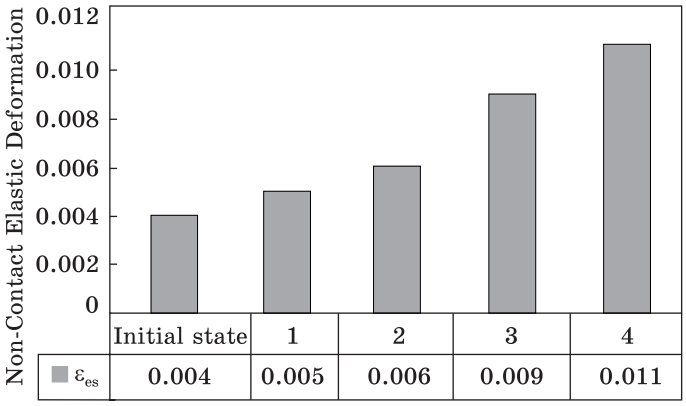

Fig. 28. Calculated values of the elastic deformation for 08пс steel in the initial hot-rolled state and after additional deformation by the THP method along the sample radius: *1* — specimen centre, *2* — middle of sample radius, *3* — sample periphery

follows: from $\varepsilon_{es} = 0.003955$ to $\varepsilon_{es} = 0.00832$ for 01ЮТА steel, while the values of $\varepsilon_{es} = 0.005018$ to $\varepsilon_{es} = 0.1085$ are detected for 01ЮТ steel. For 01ЮТ(Ca), which contains calcium, the value of ε_{es} also increases from the sample centre to its periphery: from $\varepsilon_{es} = 0.004287$ to $\varepsilon_{es} = 0.00795$; however, there is a decrease in this value found within the sample middle radius as $\varepsilon_{es} = 0.003027$.

The calculated values of the non-contact elastic deformation for 08пс-grade steel are demonstrated in Fig. 28 (hot-rolled material after additional plastic deformation by the THP methods).

The calculation of the elastic deformation values have been carried out. They vary along the radius of the sample: the minimum value in the centre is $\varepsilon_{es} = 0.004$, while the maximum one is at the periphery $\varepsilon_{es} = 0.011$. It follows that both the elastic and the plastic properties of the material, revealed by the indentation procedure, are controlled by the value of the material elastic deformation.

6.2. Determining the Ductility Characteristics of 08пс Steel and the Ultra-Low Carbon Steels in Hot-Rolled State and after THP Processing by Yu. V. Milman Methodology

Two fundamental properties can be distinguished in the physics of strength. They determine the mechanical behaviour of materials in terms of strength and plasticity. The strength of the material is determined by its ability to withstand the applied force [176]. More specifically, the strength of a solid can be defined as the resistance of a solid to tearing into two or more parts. Strength is calculated in accordance with thereof definitions when tested for tension by a destructive load

divided by the sample cross-sectional area. In physics and in engineering, plasticity is determined by the ability of the material to undergo permanent deformation under loading [178]. In the Russian conventional physics of strength and physics of plasticity, A.N. Orlov and V.R. Regel defined the plasticity as 'the properties of solid bodies to be irreversibly deformed under the influence of external forces or internal stresses' [177].

Commonly, plasticity is characterized by elongation of ductility (δ) when tested for tension or lateral narrowing of toughness (ψ) before the fracture occurs. These parameters of the material are of great practical importance, but they do not completely reflect the essence of the above definitions of plasticity. This is because they determine the conditions for the transition from a plastic deformation to destruction and do not always correlate with the definition of plasticity in the sense of the material ability to undergo the permanent deformations under load.

Thus, the parameters of δ and ψ are determined not only by plasticity, but also by, at least, two other conditions: the ratio between the yield stresses and the destructive strain, as well as the strain strengthening. The parameter of δ normally includes uniform deformation and deformation after the formation of a stable "neck" and the deformation localization within it. According to the above-mentioned physical definition, the plasticity of the material is to increase continuously with the temperature increasing since the temperature increase facilitates the movement of dislocations in solids (the exception is some intermetallides).

Therefore, it is reasonable to introduce a new characteristic of plasticity as a constituent of the plastic deformation within the general elastic-plastic deformation [179]. Such a characteristic (in accordance with the physical definition of plasticity as the ability of a material to be plastically deformed) was proposed in Ref. [180] in the form of a dimensionless parameter.

This characteristic of plasticity can be determined by various methods of mechanical testing (stretching, compression, bending), but it is easier to determine it when the tests with a pyramidal indenter, as shown in Refs. [181–183].

When indentation is over the small amounts of material being deformed, the specific character of the stress fields reduces the ability to the macroscopic destruction and dramatically reduces the temperature of cold brittleness. This makes it possible to determine the hardness and the characteristics of plasticity for most materials, even at cryogenic temperatures.

For a standard Berkovich indenter, the plasticity characteristics (δ_H) can be determined by the following expression [184]:

$$\delta_H = 1 - 10.2 \times (1 - \upsilon - 2\upsilon^2)\, HM/E, \qquad (6.5)$$

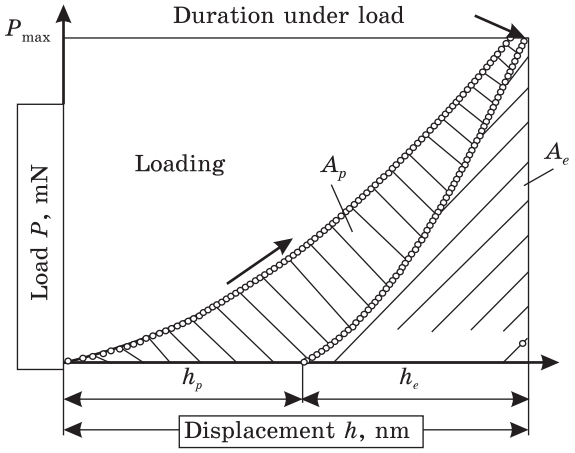

Fig. 29. Load–strain diagram of a standard Berkovich indenter in the coordinates of the load and displacement of the indenter [185]

where υ is Poisson's ratio, HM is a hardness of indentation (GPa), and E is modulus of elasticity (GPa).

The calculation of the plasticity characteristics of (δ_H) is required for the studies when the scientists address the chemical composition influence, thermal and mechanical processing and the structural state in terms of hardness, microhardness and nanohardness of materials. It can be defined as below. Uniting the characteristics of strength and those of plasticity enables a more complete description of the material mechanical behaviour than that involving only hardness phenomenon. The plasticity characteristic (δ_A) is determined in accordance with Ref. [185] and is calculated from the ratio of the planes to the continuous plasticity (δ_A) determined by the method of continuous penetration diagram (Fig. 29) by formula

$$\delta_A = \frac{A_p}{A_t} = 1 - \frac{A_e}{A_t}, \qquad (6.6)$$

where A_e is area under the unloading curve, A_t is area under the load curve, $A_p = A_t - A_e$.

The characteristics of plasticity (δ_A) determined by the method of continuous penetration, is an analogue of the dimensionless plasticity parameter (δ_H), the constituent of the plastic deformation within the general elastoplastic deformation under the indenter, which characterizes the ability of the material to formability under deformation.

The changes in the values of the plasticity characteristics of δ_H and δ_A after THP along the radius of the ultralow-carbon steel sample, calculated by formulae (6.5) and (6.6), are shown in Figs. 30 and 31. For steels of 01Ю0ТА and 01Ю0Т, the same type of change in ductility δ_H is observed: from the centre to the periphery, the plasticity characteristic of ductility is reduced (Fig. 30, *a* and *b*), which agrees with the distribution of the hardness along the radius of the sample. For the steel of

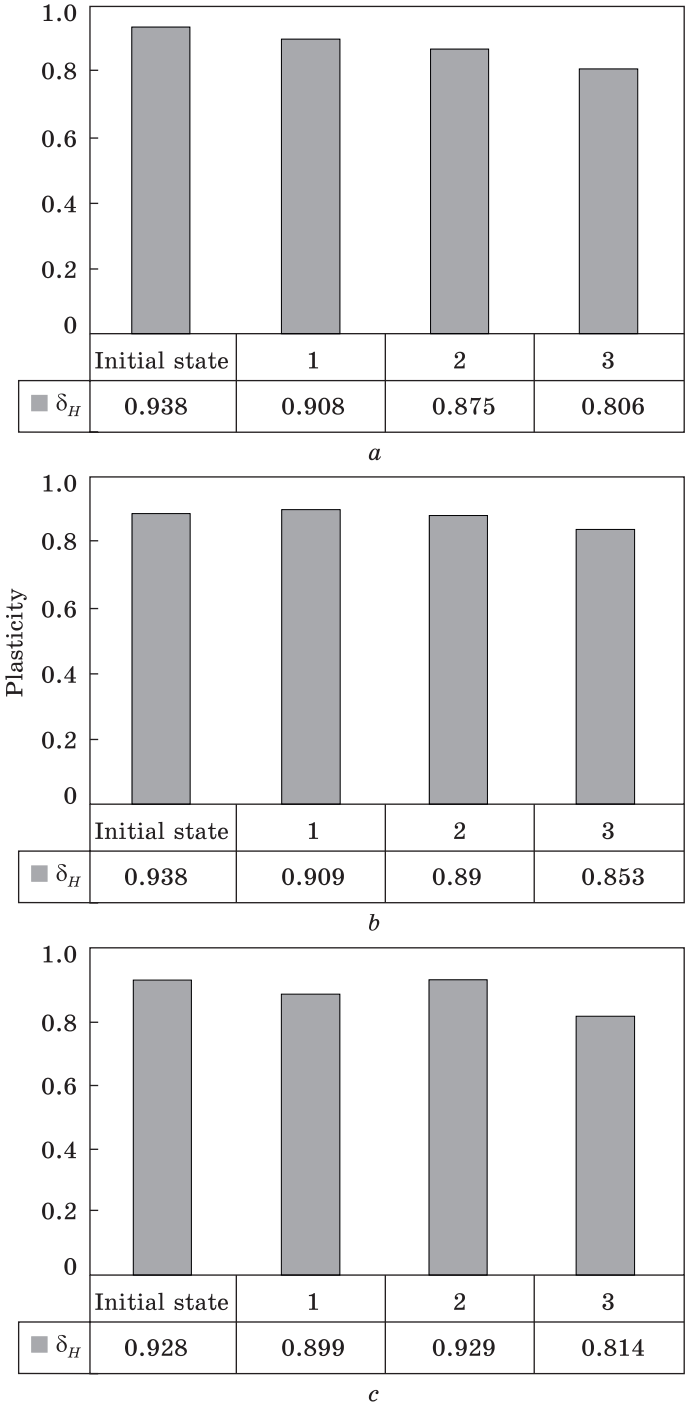

Fig. 30. Distribution of plasticity characteristics (δ_H) of the ultralow-carbon steel along the sample radius in the initial hot-rolled state and after additional strain by THP methods: *1* — sample centre, *2* — middle of sample radius, *3* — sample periphery; *a* — 01ЮТА, *b* — 01ЮТ, *c* — 01ЮТ(Ca)

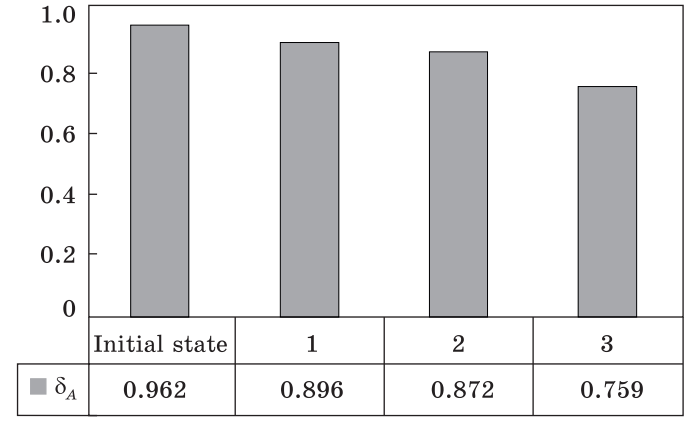

a

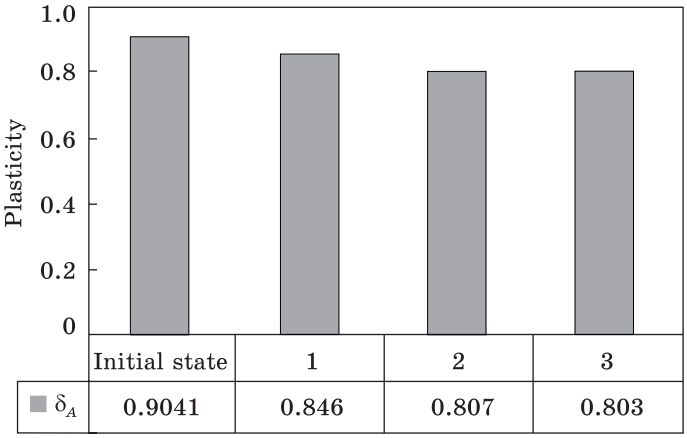

b

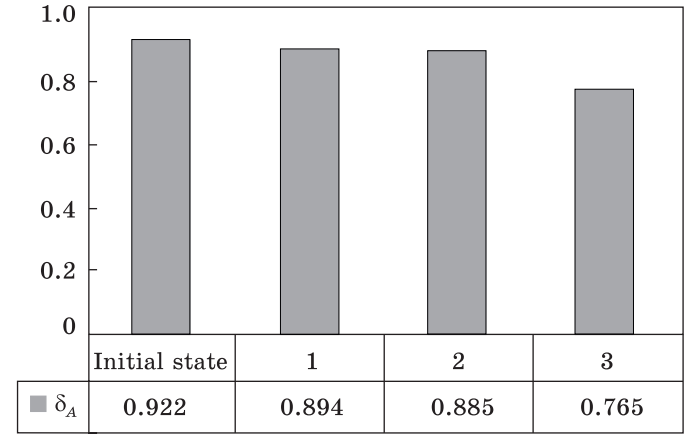

c

Fig. 31. Distribution of plasticity characteristics (δ_A) of the ultralow-carbon steel along the sample radius in the initial hot-rolled state and after additional deformation by THP methods: *1* — sample centre, *2* — middle of the sample radius, *3* — sample periphery; *a* — 01Ю0ТА, *b* — 01Ю0Т, *c* — 01Ю0Т(Ca)

01ЮТ (Ca), there is a slight change in this dependence, the plasticity of the sample middle metal is equal to the initial value, while in its centre and at its periphery the ductility is lower (Fig. 30, *c*). Despite a slight decrease in the Young modulus, the increase in the hardness at the sample periphery of the ultralow-carbon steel being studied leads to a slight decrease in the plasticity characteristics of ductility δ_H: up to 0.8–0.85 of the hot-rolled ultralow-carbon steel subjected to THP. It has been established that the ductility δ_A of the ultralow-carbon steel after THP decreases within the distance from the sample centre to its periphery. The analysis of Figs. 30 and 31 has shown a good consistency of measurement results in two plasticity characteristics (δ_H and δ_A). The maximum values of plasticity are observed in the sample central part of 01ЮТА (Fig. 30, *a*, and Fig. 31, *a*), 01ЮТ (Figs. 30, *b*, and 31, *b*), 01ЮТ(Ca) (Fig. 30, *a*, and Fig. 31, *a*). The ductility of δ_H and δ_A on the sample periphery reaches the minimum values, but the plasticity remains at a rather high level, despite the high values of its hardness. The special methods have been developed; they allow improving the ductility of nanostructural materials to some extent.

The most known methods [186] for increasing the plasticity of nanostructured materials include the following. The formation of a duplex structure consisting of nanoscale grains and a number of larger grains in which plastic deformation is initiated; the formation of nanodispersed particles of the second phase, able to cause the deformation strengthening and to increase deformation before the formation at the stable neck stretching.

The possibility to characterize quantitatively the plasticity of the ultrafine-grained ultralow-carbon steel (like other steels) opens up the possibility of finding the ways to increase the plasticity of these materials.

For the 08пс steel ($\varepsilon = 8.2\%$) in the initial state, the value of the plasticity characteristic is $\delta_H = 0.901$. The drop in the plasticity characteristics after THP processing is caused by an increase in hardness values stipulated by the surface hardening. The uneven distribution of the plasticity characteristics along the sample radius is explained by the nature of the deformation localization in the THP process at the sample periphery. For $e = 5.308$ and $H = 6.01$ GPa (corresponds to the value at the sample periphery), the ductility index is $\delta_H = 0.752$; while for $e = 3.8$ and $H = 3.4$ GPa (in the central sample zone) $\delta_H = 0.892$, which is very close to the value of the ductility index in the initial state (Fig. 32) [186].

Thus, the plasticity characteristic of δ_H is determined by the ratio of HM/E. With the increasing hardness, the value of this plasticity characteristic decreases at a constant elasticity modulus (E). Moreover, the effect of the plasticity reducing along with the hardness increasing should enhance together with the simultaneous reduction of the Young modulus.

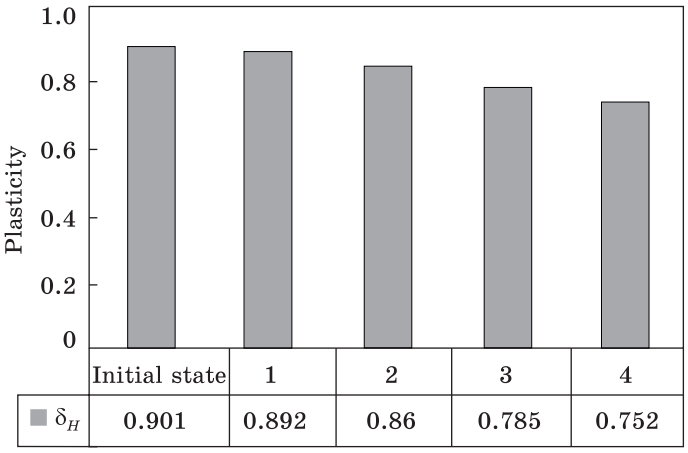

Fig. 32. Distribution of plasticity characteristics (δ_H) for 08пс steel along the sample radius in the initial hot-rolled state and after additional deformation by THP methods [186]: *1* — sample centre, *2* — middle of the sample radius, *3* and *4* — sample periphery

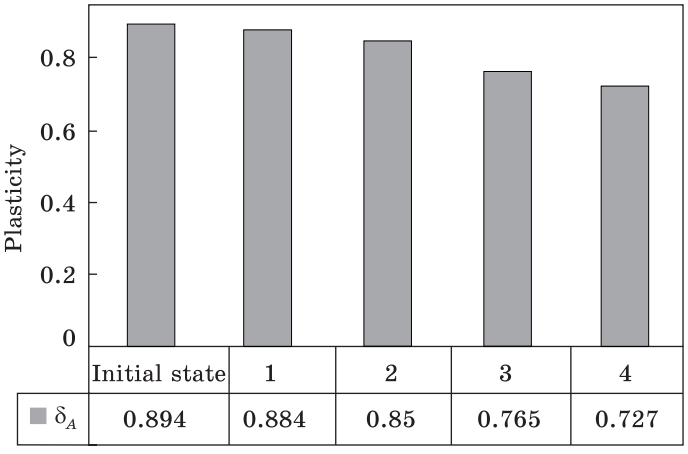

Fig. 33. Distribution of plasticity characteristics (δ_A) for 08пс steel along the sample radius in the initial hot-rolled state and after additional strain by THP methods [186]: *1* — sample centre, *2* — middle of the sample radius, *3* and *4* — sample periphery

Figure 33 illustrates the variable value of δ_A along the radius of the steel sample of 08пс. The experimental studies have shown that $\delta_H \approx \delta_A$ with the sufficient accuracy. In the initial hot-rolled state, $\delta_A = 0.894$. There is observed a drop in the plasticity along the radius of the sample from $\delta_A = 0.884$ to $\delta_A = 0.727$. At this, the plasticity δ_A is defined by formula (6.6). Unlike the method applied for δ_H, it does not require the defining of the Young modulus, the hardness and the Poisson ratio, which are able to bring some error into the calculation.

In contemporary physics of the strength and plasticity, the materials plasticity is commonly determined as the ability of the material to undergo the residual deformations under load. In practice, the material stretching until the fracture commonly characterizes the plasticity.

7. Conclusions

This review paper reports on the scientific and practical solutions of the problem, which consist in the establishment of the patterns of the structure formation, the texture formation and the formation of the mechanical properties of the low-carbon and ultralow-carbon 08пс-, 01Ю Т-, 01Ю Т(Ca)-, and 01ЮТА-grade steels at combined plastic deformation. This makes it possible to establish rational regimes of complex processing for 08пс, 01Ю Т, 01Ю Т(Ca), 01ЮТА steels to increase the complex of their mechanical properties.

Based on theoretical and experimental study, the following scientific and practical conclusions appear.

I. The analysis of the scientific and technical literature along with market demands has shown that the study of the structure of low-carbon and ultralow-carbon steels in combined deformation for improving their mechanical properties is an urgent task.

II. The effect of combined plastic deformation on the structure formation, the grain size, the dislocation density, the micro-stresses of the hot-rolled low-carbon and ultralow-carbon 08ps-, 01Ю Т-, 01Ю Т(Ca)-, and 01ЮТА-type steels has revealed as follows.

Due to the torsion under the hydrostatic pressure of the low-carbon and ultralow-carbon 08ps, 01Ю Т, 01Ю Т(Ca), and 01ЮТА steels, the nonhomogeneous structure is formed and is characterized by the metal flow in the direction of torsion. This heterogeneity is stipulated by the change of the deformation at torsion under hydrostatic pressure ($N = 5$) in the sample area from its periphery ($e = 5.867$, $\gamma = 353.250$) to its centre ($e = 4.363$, $\gamma = 78.50$).

X-ray structural analysis of the hot-rolled low and the hot-rolled ultralow carbon 08пс, 01Ю Т, 01Ю Т(Ca), and 01ЮТА steels after additional deformation by torsion under hydrostatic pressure method confirms the formation of an ultra-fine-grained structure with coherent scattering region of less than 100 nm in the (110) and (220) planes.

The value of the micro-stresses of 08ps-grade steel at torsion under hydrostatic pressure ($N = 5$) is 1.14 times higher than that in the initial state of this steel.

The density of the dislocations in the ferrite grains of steel 01Ю Т after torsion under hydrostatic pressure at $P = 300$ kgf/cm^2 and $N = 5$ increases in comparison with the initial state of this steel by 1.5 times while for the 01Ю Т(Ca) steel it makes 1.3 times, and for 01ЮТА steel

by 1.5 times. The values of micro-stresses developing within the ultralow-carbon steel unit after the torsion under hydrostatic pressure increase in comparison with the initial hot-rolled state in the 01ЮТ and 01ЮТ(Ca) steels as much as 1.13 and 1.4 times, respectively. The resulting differences are probably related to the introduction of calcium into 01ЮТ(Ca) steel, which in comparison with other alloying elements has the largest atomic radius.

III. By means of electronic microscopy and microdiffraction applied for thin foils, the fine grain boundary, the dislocation, the polygonised and the deformed structures of the low-carbon and ultralow-carbon 08пс and 01ЮТ steels have been studied and the following has been revealed.

The deformation after the hot rolling is distributed directly along the radius of the sample disk and this inhomogeneity is manifested in the dislocation-cell structure, as in the images of the fine structure, and in the microdiffraction patterns.

The electron-microscopic analyses of the hot-rolled 08пс and 01ЮТ(Ca) steels after torsion under hydrostatic pressure confirm the deformation localization at the periphery of the sample and the formation of cells of 0.5–1.0 microns in the size.

In the course of the steel hot deformation during rolling, the texture with a pronounced component {110} is being formed because of turning the body-centred cubic arrangement of the ferrite along the direction of the frictional force action due to the shear tangential friction force acting in the deformation zone within the surface layer.

In the central rolled zone, the force influence at the deformation is symmetrical, therefore the usual texture of rolling with the most expressed orientations are {100} and {111} being formed.

The additional severe plastic deformation by torsion under hydrostatic pressure method for the ultralow-carbon steel of 01ЮТ(Ca) results in the formation of the texture with {100}, {111}, and {110} components.

Inverse pole figures of the hot rolled steels of 08пс and 01ЮТ(Ca) indicate the introduction of crystallographic deformation mechanisms in the process of additional cold deformation by torsion under hydrostatic pressure method.

IV. The calculated characteristics of strength and plasticity of the low-carbon and ultralow-carbon 08пс, 01ЮТА, 01ЮТ, 01ЮТ(Ca) steels on the basis of the data obtained by the nanoindentation method have been revealed as follows.

The additional deformation for the hot-rolled steels of 01ЮТА-, 01ЮТ-, 01ЮТ(Ca)-, and 08пс-grade by torsion under hydrostatic pressure methods leads to the increase in indentation hardness both in the centre and at the periphery of the sample in 1.5–2 times.

The irregular distribution of the hardness along the radius of the sample is due to the localization of the deformation at the periphery of the sample.

Because of precipitation of 01ЮТА, 01ЮТ, 01ЮТ(Ca) steels, there is a decrease in plasticity observed with respect to the initial hot-rolled state for all samples of the investigated steels. The maximum decrease in plasticity properties is the feature for the 01ЮТ(Ca) steel: $\delta_H = 0.66$, which is 71% lower than that in the initial hot-rolled state.

In severe plastic deformation by torsion under hydrostatic pressure method, the plasticity of the hot-rolled low-carbon and ultralow-carbon steels is kept at a rather high level with respect to the initial state. The uneven distribution of the plasticity along the radius of the sample is due to the nature of the deformation localization in torsion under hydrostatic pressure processes at the sample periphery.

REFERENCES

1. D. Brandshtetter, *Tekhnologiya otzhiga v kolpakovykh pechakh. Sovremennye kontseptsii proizvodstva kholodnokatanoy tonkolistovoy stali dlya avtomobilestroeniya* [The annealing technology in bell-type furnaces. The modern concepts for the production of cold rolled sheet steel for the automotive industry], Trudy IV Kongressa prokatchikov (Moscow: 2002), p. 227 (in Russian).
2. State Standard 1997.01.01. *Prokat tonkolistovoy kholodnokatanyy iz nizkouglerodistoy kachestvennoy stali dlya kholodnoy shtampovki*. Tekhnicheskie usloviya: ГОСТ 9045-93 [The cold-rolled thin sheet steel from the low-carbon quality steel for cold press forming. Technical conditions: ГОСТ 9045-93] (Minsk: Izdatel'stvo standartov: 1993), p. 10 (in Russian).
3. O.N. Yakubovskiy, *Proizvodstvo Prokata*, Nos. 11–12: 30 (1998) (in Russian).
4. V. Blek, R. Brode, and A. Fel'd, *Chernyye Metally*, No. 8: 19 (1994) (in Russian).
5. V.K. Potemkin, O.S. Khlybov, and A.V. Kusaylo, *Byulleten' 'Chernaya Metallurgiya'*, No. 2: 43 (2002) (in Russian).
6. X. Takeshi, *Sovremennye dostizheniya v metallurgii i tekhnologii proizvodstva staley dlya avtomobil'noy promyshlennosti: Mezhdunarodnyy seminar* [Modern advances in metallurgy and steel production technology for the automotive industry: International seminar] (Moscow: I.P. Bardin TsNIICherMet: 2004) (in Russian).
7. E.T. Ruoff, *Chernye Metally*, No. 10: 44 (2000) (in Russian).
8. A.V. Protasov, A.I. Mayorov, and I.V. Komolov, *Byulleten' 'Chernaya Metallurgiya'*, No. 2: 58 (2006) (in Russian).
9. Yu.V. Lipukhin, V.I. Slavov, and V.V. Kuznetsov, *Stal'*, No. 3: 63 (1993) (in Russian).
10. A.A. Stepanov, S.D. Zinchenko, and A.M. Lamukhin, *Byulleten' 'Chernaya Metallurgiya'*, No. 1: 39 (2005) (in Russian).
11. S. D. Zinchenko, S.V. Efimov, and M.V. Filatov, *Byulleten' 'Chernaya Metallurgiya'*, No. 5: 32 (2005) (in Russian).
12. R. Pradhan, *IFS-IF'94*: 165 (1994).

13. H. Takechi, *Iron and Steel Institute of Japan International*, **34**, No. 1: 1 (1994).
14. A. Yungraytmayer, E. Pissenberger, and K. Burgshtaller, *Novosti Chernoy Metallurgii za Rubezhom*, No. 5: 32 (2004) (in Russian).
15. B.F. Zin'ko, A.A. Stepanova, and A.V. Izotov, *Sovremennyye dostizheniya v metallurgii i tekhnologii proizvodstva staley dlya avtomobil'noy promyshlennosti: Mezhdunarodnyy seminar* [Modern advances in metallurgy and steel production technology for the automotive industry: International seminar] (Moscow: I. P. Bardin TsNIICherMet: 2004) (in Russian).
16. A.I. Longinov, I.A. Petushkov, and S.V. Efimov, *Metallurg*, No. 12: 42 (2005) (in Russian).
17. F. Khaysterkampf, K. Khulka, and Yu.I. Matrosov, *Niobiysoderzhashchie nizkolegirovannye stali* [Niobium-containing low alloy steels] (Moscow: SP–Intermet inzheniring: 1999) (in Russian).
18. Ts. Nagamiti, M. Midzumi, and A. Okamoto, *Novosti Chernoy Metallurgii za Rubezhom*, No. 1: 100 (1997) (in Russian).
19. A. Itami, K. Ushioda, and N. Kimura, *Novosti Chernoy Metallurgii za Rubezhom*, No. 3: 89 (1996) (in Russian).
20. State Standard 1980.01.01. *Prokat iz kachestvennoy konstruktsionnoy uglerodistoy i legirovannoy stali dlya kholodnogo vydavlivaniya i vysadki*. Tekhnicheskie usloviya: ГОСТ 10702-78 [The rolled quality carbon structural and alloyed steel for cold extrusion and upsetting. Technical conditions: ГОСТ 10702-78] (Moscow: Izdatel'stvo ofitsial'noe: 2006) (in Russian).
21. A.N. Bryukhanov, *Kovka i ob'emnaya shtampovka: uchebnoe posobie* [Forging and bulk press forming] (Moscow: Mashinostroenie: 1975) (in Russian).
22. A.Yu. Averkiev, *Kovka i shtampovka: spravochnik v 4-kh tomakh* [Forging and press forming] (Moscow: Mashinostroenie: 1985) (in Russian).
23. Ya.M. Okhrimenko, *Tekhnologiya kuznechno-shtampovochnogo proizvodstva: uchebnik* [Technology of forging and stamping production: a textbook] (Moscow: Mashinostroenie: 1976) (in Russian).
24. V.M. Segal, V.I. Reznikov, and V.I. Kopylov, *Protsessy plasticheskogo strukturoobrazovaniya metallov* [Processes of plastic structure formation of metals] (Moscow: Nauka i tekhnika: 1994) (in Russian).
25. R.Z. Valiev and I.V. Aleksandrov, *Nanostrukturnye materialy, poluchennye intensivnoy plasticheskoy deformatsiey* [Nanostructured materials obtained by severe plastic deformation] (Moscow: Logos: 2000) (in Russian).
26. Ya.E. Beygel'zimer, V.N. Varyukhin, D.V. Orlov, and S.G. Synkov, *Vintovaya ekstruziya — Protsess nakopleniya deformatsii* [Spiral extrusion — Deformation accumulation process] (Donetsk: TEAN: 2003) (in Russian).
27. Ya.E. Beygel'zimer and N.M. Lavrinenko, *Naukovi Notatki*, **39**: 8 (2012) (in Russian).
28. Yu.A. Bykov and S.D. Karpukhin, *Nanoinzheneriya*, No. 6: 11 (2012) (in Russian).
29. Y.T. Zhu, T.G. Langdon, R.Z. Valiev, S.L. Semiatin, D.H. Shin, and T.C. Lowe, *Ultrafine grained materials III. Charlotte* (North Carolina: TMS: 2004).
30. Y.T. Zhu, T.G. Langdon R.S. Mishra, S.L. Semiatin, M.J. Saran, and T.C. Lowe, *Ultrafine grained materials II* (Seattle (WA): TMS: 2002).
31. Y.T. Zhu, T.G. Langdon, Z. Horita, M. Zehetbauer, S.L. Semiatin, and T.C. Lowe, *Ultrafine grained materials IV* (San Antonio (Texas): TMS: 2006).
32. Y. Estrin and H.J. Maier, Nanomaterials by severe plastic deformation IV (Zurich: TransTech: 2008).

33. J.T. Wang, R.B. Figueiredo, and T.G. Langdon, *Nanomaterials by severe plastic deformation* (Zurich: TransTech: 2011).
34. G. Sha, Y.B. Wang, X.Z. Liao, Z.C. Duan, S.P. Ringer, and T.G. Langdon, *Acta Mater.*, **57**: 3123 (2009). https://doi.org/10.1016/j.actamat.2009.03.017
35. D. Jia, K.T. Ramesh, and E. Ma, *Acta Mater.*, **51**: 3333 (2003). https://doi.org/10.1016/S1359-6454(03)00169-1
36. L.J. Kecskes K.C. Cho, R.J. Dowding, B.E. Schuster, R.Z. Valiev, and Q. Wei, *Mater. Sci. Eng. A*, **467**: 33 (2007). https://doi.org/10.1016/j.msea.2007.02.099
37. R. Song, D. Ponge, D. Raabe, J.G. Speer, and D.K. Matlock, *Mater. Sci. Eng. A*, **441**: 1 (2006). https://doi.org/10.1016/j.msea.2006.08.095
38. X.Z. Liao, J.Y. Huang, Y.T. Zhu, F. Zhou, and E.J. Lavernia, *Phil. Mag.*, **83**: 3065(2003). https://doi.org/10.1080/1478643031000152799
39. N. Hansen, *Met. Mater. Trans.*, **32**: 2917 (2001). https://doi.org/10.1007/s11661-001-0167-x
40. D.A. Hughes and N. Hansen, *Acta Mater.*, **45**: 3871 (1997). https://doi.org/10.1016/S1359-6454(97)00027-X
41. L. Bracke, K. Verbeken, L. Kestens, and J. Penning, *Acta Mater.*, **57**: 1512 (2009). https://doi.org/10.1016/j.actamat.2008.11.036
42. I. Gutierrez-Urrutia and D. Raabe, *Acta Mater.*, **59**: 6449 (2011). https://doi.org/10.1016/j.actamat.2011.07.009
43. Y.B. Wang, X.Z. Liao, Y.H. Zhao, E.J. Lavernia, S.P. Ringer, Z. Horita, T.G. Langdon, and Y.T. Zhu, *Mater. Sci. Eng. A*, **527**: 4959 (2010). https://doi.org/10.1016/j.msea.2010.04.036
44. X.H. An, Q.Y. Lin, S. Qu, G. Yang, S.D. Wu, and Z.F. Zhang, *J. Mater. Res.*, **24**: 3636 (2009). https://doi.org/10.1557/jmr.2009.0426
45. C.S. Hong, N.R. Tao, X. Huang, and K. Lu, *Acta Mater.*, **58**, No. 8: 3103 (2010). https://doi.org/10.1016/j.actamat.2010.01.049
46. J.A. Venables, *Phil. Mag.*, **6**: 379 (1961). https://doi.org/10.1080/14786436108235892
47. S. Mahajan and G.Y. Chin, *Acta Metall.*, **21**: 1353 (1973). https://doi.org/10.1080/14786435.2016.1240379
48. S. Mahajan, *Scr. Mater.*, **68**: 95 (2013). https://doi.org/10.1016/j.scriptamat.2012.09.011
49. B. Cohen and J. Weertman, *Acta Metall.*, **11**: 996 (1963). https://doi.org/10.1016/0001-6160(63)90074-9
50. H. Fujita and T. Mori, *Scr. Metall.*, **9**, No. 6: 631 (1975). https://doi.org/10.1016/0036-9748(75)90476-7
51. M. Niewczas and G. Saada, *Philos. Mag.*, **82**: 167 (2002). https://doi.org/10.1080/01418610208240003
52. J.W. Christian and S. Mahajan, *Prog. Mater. Sci.*, **39**: 157 (1995). https://doi.org/10.1016/0079-6425(94)00007-7
53. J. Wang, N.Li, O. Anderoglu, X. Zhang, A. Misra, J.Y. Huang, and J.P. Hirth, *Acta Mater.*, **58**: 2262 (2010). https://doi.org/10.1016/j.actamat.2009.12.013
54. Y. Zhang, N.R. Tao, and K. Lu, *Scr. Mater.*, **60**: 211 (2009). https://doi.org/10.1016/j.scriptamat.2008.10.00
55. Y. Cao, Y.B. Wang, Z.B. Chen, X.Z. Liao, M. Kawasaki, S.P. Ringer, T.G. Langdon, and Y.T. Zhu, *Mater. Sci. Eng. A*, **578**: 110 (2013). https://doi.org/10.1016/j.msea.2013.04.075

56. S.Ni, Y.B. Wang, X.Z. Liao, R.B. Figueiredo, H.Q. Li, S.P. Ringer, T.G. Langdon, and Y.T. Zhu, *Acta Mater.*, **60**: 3181 (2012). https://doi.org/10.1016/j.actamat.2012.02.026
57. A.M. Hodge, T.A. Furnish, C.J. Shute, Y. Liao, X. Huang, C.S. Hong, Y.T. Zhu, T.W. Barbee, and J.R. Weertman, *Scr. Mater.*, **66**: 872 (2012). https://doi.org/10.1016/j.scriptamat.2012.01.027
58. C.J. Shute, B.D. Myers, S. Xie, S.Y. Li, T.W. Barbee, A.M. Hodge, and J.R. Weertman, *Acta Mater.*, **59**: 4569 (2011). https://doi.org/10.1016/j.actamat.2011.04.002
59. Y. Wei, *Mater. Sci. Eng.*, **528**: 1558 (2011). https://doi.org/10.1016/j.msea.2010.10.072
60. O. Anderoglu, A. Misra, J. Wang, R.G. Hoagland, J.P. Hirth, and X. Zhang, *Int. J. Plasticity*, **26**: 875 (2010). https://doi.org/10.1016/j.ijplas.2009.11.003
61. R.Z. Valiev, Annales de Chimie, *Science des Materiaux*, **21**, No. 6: 369 (1996). https://doi.org/10.1007/978-1-84882-454-6_19
62. M. Furukawa, Z. Horita, M. Nemoto, and T.G. Langdon, Mater. *Sci. Eng. A*, **324**: 82 (2002). https://doi.org/10.1016/S0921-5093(01)01288-6
63. A. Vorhauer, R. Pippan, M.J. Zehetbauer, and R.Z. Valiev, *Conf. Nanomaterials by Severe Plastic Deformation: Fundamentals–Processing–Application* (Vienna: 2002), p. 684.
64. C. Xu, Z. Horita, and T. G. Langdon, *Acta Mater.*, **56**: 5168 (2008). https://doi.org/10.1016/j.actamat.2008.06.036
65. T.G. Langdon, *Acta Mater.*, **61**: 7035 (2013). https://doi.org/10.1016/j.actamat.2013.08.018
66. G. Salishchev, R. Imayev, V. Imayev, N. Gabdullin, M. Shagiev, A. Kuznetsov, O.N. Senkov, and F.H. Froes, *Investigations and Applications of Severe Plastic Deformation*. NATO Science Series (Series 3. High Technology) (Eds. T.C. Lowe and R.Z. Valiev), Vol. **80** (Dordrecht: Springer: 2000), p. 49. https://doi.org/10.1007/978-94-011-4062-1_7
67. R.I. Kuznetsov, V.I. Bykov, V.P. Chernyshev, V.P. Pilyugin, N.A. Efremov, and A.V. Pasheev, *Plasticheskaya deformatsiya tverdykh tel pod davleniem: monografiya* [Plastic deformation of solids under pressure: monograph] (Sverdlovsk: IFMURO Akademii nauk SSSR: 1985) (in Russian).
68. D.I. Tupitsa, V.P. Pilyugin, R.I. Kuznetsov, G.G. Taluts, and V.A. Teplov, *Fiz. Met. Metalloved.*, **61**, No. 2: 325 (1986) (in Russian).
69. N.A. Smirnova, V.I. Levit, V.I. Pilyugin, R.I. Kuznetsov, L.S. Davydova, and V.A. Sazonov, *Fiz. Met. Metalloved.*, **61**: 1170 (1986) (in Russian).
70. N.A. Smirnova, V.I. Levit, V.P. Pilyugin, R.I. Kuznetsov, and M.V. Degtyarev, *Fiz. Met. Metalloved.*, **62**: 566 (1986) (in Russian).
71. V.A. Teplov, V.P. Pilyugin, R.I. Kuznetsov, D.I. Tupitsa, V.A. Shabashov, and V.M. Gundyrev, *Fiz. Met. Metalloved.*, **64**, No. 1: 93 (1987) (in Russian).
72. A.P. Zhilyaev, G.V. Nurislamova, B.K. Kim, M.D. Bar, J.A. Szpunar, and T.G. Langdon, *Acta Mater.*, **51**: 753 (2003). https://doi.org/10.1016/j.jallcom.2016.07.149
73. A.P. Zhilyaev, S. Lee, G.V. Nurislamova, R.Z. Valiev, and T.G. Langdon, *Scr. Mater.*, **44**: 2753 (2001). https://doi.org/10.1016/S1359-6462(01)00955-1
74. R.Z. Valiev, Yu.V. Ivanisenko, E.F. Rouch and B. Boudelet, *Acta Mater.*, **44**: 4705 (1996). https://doi.org/10.1016/S1359-6454(96)00156-5
75. M.L. Bernshteyn, *Struktura deformirovannykh metallov* [Structure of the deformed metals] (Moscow: Metallurgiya: 1977) (in Russian).

76. A. Vorhauer and R. Pippan, *Scr. Mater.*, **51**: 921 (2004). https://doi.org/10.1016/j.scriptamat.2004.04.025
77. T. Hebesberger, H.P. Stewe, A. Vorhauer, F. Wetscher, and R. Pippan, *Acta Mater.*, **53**: 393 (2005). https://doi.org/10.1016/j.actamat.2004.09.043
78. R. Pippan, F. Wetscher, M. Hafok, A. Vorhauer, and I. Sabirov, *Adv. Eng. Mater.*, **8**: 1046 (2006). https://doi.org/10.1002/adem.200600133
79. V.A. Pavlov, O.V. Antonov, A.P. Adakhovskiy, A.A. Kuranov, V.M. Alyab'ev, and A.I. Deryagin, *Fiz. Met. Metalloved.*, **58**: 177 (1984) (in Russian).
80. V.A. Tatarenko, S.M. Bokoch, V.M. Nadutov, T.M. Radchenko, and Y.B. Park, *Defect Diffus. Forum*, **280–281**: 29 (2008). https://doi.org/10.4028/www.scientific.net/DDF.280-281.29
81. Y. Ivanisenko, R.K. Wunderlich, R.Z. Valiev, and H.J. Fecht, *Scr. Mater.*, **49**: 947 (2003). https://doi.org/10.1016/S1359-6462(03)00478-0
82. Y. Ivanisenko, W. Lojkowski, R.Z. Valiev, and H.J. Fecht, *Acta Mater.*, **51**, No. 18: 5555 (2003). https://doi.org/10.1016/S1359-6454(03)00419-1
83. A. Vorhauer, S. Kleber, and R. Pippan, *Microstructure of Austenitic and Ferritic Steels Produced by Severe Plastic Deformation and Subsequent Annealing* (Charlotte: Ultrafine Grained Materials III, TMS: 2004).
84. A.A. Zakirova, R.G. Zaripova, and V.I. Semenov, *Vestnik UGATU*, **11**, No. 29: 123 (2008) (in Russian).
85. R. Pippan, F. Wetscher, M. Hafok, A. Vorhauer, and I. Sabirov, *Adv. Eng. Mater.*, **8**: (2006). https://doi.org/10.1002/adem.200600133
86. V.A. Pavlov, O.V. Antonov, A.P. Adakhovskiy, A.A. Kuranov, V.M. Alyab'ev, and A.I. Deryagin, *Fiz. Met. Metalloved.*, **58**: 177 (1984) (in Russian).
87. Y. Ivanisenko, R.Z. Valiev, W. Lojkowski, A. Grob, and H.J. Fecht, *Nanostructure Formation and Carbides Dissolution in Rail Steel Deformed by High Pressure Torsion* (Seattle: Ultrafine Grained Materials II, TMS: 2002).
88. Y.Y. Ivanisenko, R.K. Wunderlich, R.Z. Valiev, and H.J. Fecht, *Scr. Mater.*, **49**: 947 (2003). https://doi.org/10.1016/S1359-6462(03)00478-0
89. R.Z. Valiev, *Nanostrukturirovanie materialov intensivnoy plasticheskoy deformatsiey dlya dostizheniya perspektivnykh svoystv* [Nanostructuring of the materials by intensive plastic deformation to achieve promising properties] (Magnitogorsk: Dom Pechati: 2006), Vol. **1**, No. 4, p. 215 (in Russian).
90. A. Rollet, F.J. Humphreys, G.S. Rohrer, and M. Hatherly, *Recrystallization and Related Annealing Phenomena*, 2nd Edition (Oxford: Pergamon: 2004).
91. Nanotribology and Nanomechanics II. *Nanotribology, Biomimetics, and Industrial Applications* (Ed. B. Bhushan), (Berlin, Heidelberg: Springer: 2011). https://doi.org/10.1007/978-3-642-15263-4
92. L.Ts. Zayats, D.O. Panov, and M.G. Zakirova, *Metallovedenie i Termicheskaya Obrabotka Metallov*, No. 10: 18 (2008) (in Russian).
93. L.T. Zayats, D.O. Panov, and M.G. Zakirova, *Met. Sci. Heat Treat.*, **50**, Nos. 9–10: 473 (2008). https://doi.org/10.1007/s11041-009-9091-2
94. R.I. Kuznetsov, V.I. Bykov, V.P. Chernyshev, V.P. Pilyugin, N.A. Yefremov, and A.V. Pasheev, *Plasticheskaya deformaciya tverdyh tel pod davleniem* [Plastic deformation of solids under pressure] (Sverdlovsk: IFM URO AS USSR: 1985) (in Russian).
95. S.A. Krokhmal' and G.N. Tolmacheva, *Fizicheskaya Inzheneriya Poverkhnosti*, **9**, No. 4: 350 (2011) (in Russian).
96. ISO 14577-1:2002. Metallic materials – *Instrumented indentation test for hardness and materials parameters – Part 1: Test method*.

97. S.A. Firstov and T.G. Rogul', *Dopovidi NAN Ukrainy*, No. 4: 110 (2007) (in Russian).
98. Yu.V. Milman, *J. Physcis D*: *Appl. Phys.*, **41**: 074013 (2008). https://doi.org/10.1088/0022-3727/41/7/074013
99. State Standard 01.01.1983. *Shkurka shlifoval'naya bumazhnaya*. Tekhnicheskie usloviya: ГОСТ 6456-82 [Sanding paper Technical conditions: ГОСТ 6456-82] (Moscow: Izdatel'stvo standartov: 1990), p. 12 (in Russian).
100. State Standard 01.01.1977. *Izmerenie mikrotverdosti vdavlivaniem almaznykh nakonechnikov*. ГОСТ 9450-76 [Measurement of microhardness by indentation of diamond tips. ГОСТ 9450-76] (Moscow: Izdatel'stvo standartov: 1993), p. 34 (in Russian).
101. G.M. Eskina and V.P. Morozov, *Rentgenograficheskiy fazovyy analiz: uchebno-metodicheskoe posobie* [X-ray phase analysis: a teaching workbook] (Kazan: Kazan State University: 2010) (in Russian).
102. Ya.S. Umanskiy, Yu.S. Skakov, A.N. Ivanov, and L.N. Rastorguev, *Kristallografiya, rentgenografiya i elektronnaya mikroskopiya* [Crystallography, x-ray and electron microscopy] (Moscow: Metallurgiya: 1982) (in Russian).
103. B.E. Warren, X-Ray Diffraction (New York: Dover Publ. Inc.: 1990).
104. V.K. Pecharsky and P.Y. Zavalij, *Fundamentals of Powder Diffraction and Structural Characterization of Material* (Boston, MA: Springer: 2009). https://doi.org/10.1007/978-0-387-09579-0
105. V.A. Tatarenko and T.M. Radchenko, *Intermetallics*, **11**, Nos. 11–12: 1319 (2003). https://doi.org/10.1016/S0966-9795(03)00174-2
106. B.E. Warren and B.L. Averbach, *J. Appl. Phys.*, **23**: 497 (1952). https://doi.org/10.1063/1.1702234
107. Ya.S. Umanskiy, *Rentgenografiya metallov* [Metal Radiography] (Moscow: Metallurgiya: 1967) (in Russian).
108. B.L. Averbach and B.E. Warren, *J. Appl. Phys.*, **21**: 55 (1950). https://doi.org/10.1063/1.1699713
109. R.K. Nandi, H.K. Kuo, W. Schlosberg, G. Wissler, and J.B. Cohen, *J. Appl. Crystallogr.*, **17**: 22 (1984). https://doi.org/10.1107/S0021889884010943
110. W.H. Schlosberg and J.B. Cohen, *J. Appl. Crystallogr.*, **16**: 304 (1983). https://doi.org/10.1107/S0021889883010481
111. R. Delhez, Th.H. de Keijser, and E.J. Mittemeijer, *Z. Anal. Chem.*, **312**, No. 1: 1 (1982). https://doi.org/10.1007/BF00482725
112. J.I. Langford and A.J.C. Wilson, *J. Appl. Crystallogr.*, **11**: 102 (1978). https://doi.org/10.1107/S0021889878012844
113. V.Z. Kutsova, V.F. Balakin, G.P. Stetsenko, and T.V. Kotova, *Metaloznavstvo ta Termichna Obrobka Metaliv*, **1**: 41 (2017) (in Russian).
114. W.H. Schlosberg and J.B. Cohen, *J. Appl. Crystallogr.*, **16**: 304 (1983). https://doi.org/10.1107/S0021889883010481
115. R. Delhez, Th.H. de Keijser, and E.J. Mittemeijer, *J. Physics E: Sci. Instrum.*, **11**, No. 7: 649 (1978). https://doi.org/10.1088/0022-3735/11/7/015
116. J.I. Langford and A.J. C. Wilson, *J. Appl. Crystallogr.*, **11**: 102 (1978). https://doi.org/10.1107/S0021889878012844
117. V.Z. Kutsova, T.V. Kotova, and G.P. Ploshenko, *Innovatsiyniy potentsial svitovoi nauky – XXI storichchya* (Zaporizhzhya: 2013), vol. **2**, p. 66 (in Russian).
118. V.Z. Kutsova, T.V. Kotova, and G.P. Ploshenko, *Metalurgiina ta Girnychorudna Promyslovist'*, No. 3: 75 (2014) (in Russian).

119. Yu.A. Geller, *Materialovedenie. Metody analiza, laboratornye raboty i zadachi* [Materials Science. Analysis methods, laboratory work and problems] (Moscow: Metallurgiya: 1984) (in Russian).
120. V.L. Pilyushenko, B.B. Vinokur, and S.E. Kondratyuk, *Spravochnik po prakticheskomu metallovedeniyu* [Handbook on practical metal science] (Kiev: Tekhnika: 1984) (in Russian).
121. V.K. Barziy, *Stal'*, No. 11: 1013 (1959) (in Russian).
122. State Standard 2000.01.01. *Prokat tonkolistovoy iz uglerodistoy stali kachestvennoy i obyknovennogo kachestva obshchego naznacheniya*. Tekhnicheskie usloviya: ГОСТ 16523-97. [Rolled sheets of carbon steel of high quality and ordinary quality of general purpose. Technical conditions: ГОСТ 16523-97] (Moscow: Izdatel'stvo standartov: 1997) (in Russian).
123. Yu.M. Lakhtin and V.P. Leont'eva, *Materialovedenie: uchebnik dlya vuzov* [Materials science: a textbook for high schools] (Moscow: Mashinostroenie: 1990) (in Russian).
124. V.Z. Kutsova, G.P. Ploshenko, T.V. Kotova, G. Diya, and A. Kawalek, N*aukovi visti. Suchasni problemy metalurgii*, No. 18: 21(2015) (in Russian).
125. State Standard Stal' 31.10.1968. *Metallograficheskiy metod otsenki mikrostruktury listov i lenty*. ГОСТ 5640-68. [Steel. Metallographic method for evaluation of sheet and tape microstructure. ГОСТ 5640-68] (Moscow: Izdatel'stvo standartov: 1988) (in Russian).
126. S.V. Rzhevskaya, *Materialovedenie: uchebnik dlya vuzov* [Materials Science: a textbook for high schools] (Moscow: Logos: 2006) (in Russian).
127. I.Yu. Litovchenko, A.N. Tyumentsev, N.V. Shevchenko, and A.V. Korznikov, *Fiz. Met. Metalloved.*, **112**, No. 4: 436 (2011) (in Russian).
128. HSLA Steels: Processing, Properties and Applications (Ed. G. Tither) (Warrendale, PA: TMS: 1992).
129. J. Deloach and R. Dinale, *Welding and Weld Automation in Shipbuilding* (Warrendale, PA: TMS: 1996).
130. V.N. Rybin, *Problemy Materialovedeniya*, **29**, No. 1: 11 (2002) (in Russian).
131. V.V. Rybin, *Bol'shie plasticheskie deformatsii i razrushenie metallov* [Large plastic deformation and destruction of metals] (Moscow: Metallurgiya: 1986) (in Russian).
132. G.A. Kunitsyn, A.P. Budanov, and V.L. Kornilov, *Metallurg*, No. 1: 57 (2007) (in Russian).
133. V. Titov, *Natsiona'naya Metallurgiya*, No. 5: 84 (2004) (in Russian).
134. V. Dedek, *Polosovaya stal' dlya glubokoi vytiazhki* [Deep drawn strip steel] (Moscow: Metallurgiya: 1970) (in Russian).
135. V.M. Kosevich, V.M. Ivlev, L.S. Palatnik, and A.I. Fedorenko, *Struktura mezhkristallitnykh i mezhfaznykh granits* [Structure of intercrystalline and interphase boundaries] (Moscow: Metallurgiya: 1980) (in Russian).
136. Ch.V. Kopetskiy, A.N. Orlov, and L.K. Fionova, *Granitsy zeren v chistykh materialakh* [Grain boundaries in pure materials] (Moscow: Nauka: 1987) (in Russian).
137. M.V. Grabskiy, *Struktura granits zeren v metallakh* [The structure of the grain boundaries in metals] (Moscow: Metallurgiya: 1972) (in Russian).
138. S.Yu. Mironov, V.N. Danilenko, and M.M. Myshlyaev, *Fiz. Tverd. Tela*, **47**: 1217 (2005) (in Russian).
139. V.Z. Kutsova, O.Yu. Putnoki, T.V. Kotova, V.G. Ivanchenko, and G.P. Ploshenko, *Novini Nauky Pridniprov'ya*, No. 2: 189 (2012) (in Ukrainian).

140. V.N. Gridnev, V.G. Gavrilyuk, and Yu.Ya. Meshkov, *Prochnost' i plastichnost' kholodnodeformirovannoy stali* [Strength and ductility of cold-rolled steel] (Kiev: Naukova dumka: 1974) (in Russian).
141. V.V. Astanin, *Fiz. Met. Metalloved.*, **79**, No. 3: 166 (1995) (in Russian).
142. Yu.Ya. Meshkov and T.N. Serditova, *Razrushenie deformirovannoy stali* [Destruction of deformed steel] (Kyiv: Naukova dumka: 1989) (in Russian).
143. Yu.A. Meshkov and G.A. Pakharenko, *Struktura metalla i khrupkost' stal'nykh izdeliy* [Metal structure and brittleness of steel products] (Kyiv: Naukova dumka: 1985) (in Russian).
144. V.A. Skudnov, *Predel'nye plasticheskie deformatsii metallov* [Ultimate plastic strains of metals] (Moscow: Metallurgiya: 1988) (in Russian).
145. Yu. Projdak, V. Kutsova, T. Kotova, G. Stetsenko, H. Dyja, and A. Kawalek, *New technologies and achievements in metallurgy, material engineering, production engineering and physics. A collective monograph. Series: Monografie*, No. 68: 247 (2017) (in Russian).
146. S.P. Efimenko, *Stal'*, No. 3: 35 (2001) (in Russian).
147. M.V. Kostina, A.V. Dymov, and V.M. Blinov, *Metallovedenie i Termicheskaya Obrabotka Metallov*, No. 1: 1 (2002) (in Russian).
148. V.G. Geshelin and A.F. Osipov, *Metallurgicheskaya i gornorudnaya promyshlennost'*, No. 5: 41 (2000) (in Russian).
149. S.N. Kaverina, E.P. Pechkovskiy, G.F. Sarzhan, and S.A. Firstov, *Metallofiz. Noveishie Tekhnol.*, **24**, No. 2: 251 (2002) (in Russian).
150. R.S. Mishra, T.R. Bieler, and A.K. Mukherjee, *Acta Mater.*, **45**, No. 2: 561 (1997). https://doi.org/10.1016/S1359-6454(96)00194-2
151. N.N. Malinin, *Prikladnaya teoriya plastichnosti i polzuchesti* [Applied theory of plasticity and creep] (Moscow: Mashinostroenie: 1975) (in Russian).
152. S.E. Aleksandrov and E.A. Lyamina, *Metally*, No. 2: 94 (2002) (in Russian).
153. I.L. Yakovleva, D.A. Mirzaev, and V.M. Schastlivtsev, *Fazovye i Strukturnye Prevrashcheniya v Stalyakh*, **1**: 116 (2000) (in Russian).
154. V.M. Schastlivtsev, D.A. Mirzaev, and I.L. Yakovleva, *Perlit v uglerodistykh stalyakh* [Perlite in carbon steels] (Ekaterinburg: UrO RAN: 2006) (in Russian).
155. V.Z. Kutsova, T.V. Kotova, G.P. Ploshenko, and Z. Stadomski, *Metallurgy*. 2013: New Technologies and Achievements: A Collective Monograph, **2**, No. 31: 65 (2013) (in Russian).
156. O.N. Shtekhno, B.N. Fogel', and G.V. Levchenko, *Stal'*, No. 10: 62 (2003) (in Russian).
157. G.V. Levchenko, A.M. Nesterenko, A.V. Yankovskiy, and S.A. Vorobey, *Teoriya i Praktika Metallurgii*, Nos. 1–2: 85 (2005) (in Russian).
158. A. Belevitin, V.F. Obesnyuk, and E.R. Logunova, *Metally*, No. 1: 26 (2003) (in Russian).
159. B.S. Bokshteyn, Ch.V. Kopetskiy, and L.S. Shvindlerman, *Termodinamika i kinetika granits zeren v metallakh* [Thermodynamics and kinetics of grain boundaries in metals] (Moscow: Metallurgiya: 1986) (in Russian).
160. Ch.V. Kopetskiy, A.N. Orlov, and L.K. Fionova, *Granitsy zeren v chistykh materialakh* [Grain boundaries in pure materials] (Moscow: Nauka: 1987) (in Russian).
161. I.P. Kudryavtsev, *Tekstury v metallakh i splavakh* [Textures in metals and alloys] (Moscow: Metallurgiya: 1965) (in Russian).

162. V.I. Bol'shakov, G.D. Sukhomlin, and D.V. Laukhin, *Theoretical Foundation of Civil Engineering: Polish–Ukrainian–Lithuaninan Transactions*, **15**: 73 (2007) (in Russian).
163. Ya.D. Vishnyakov, A.A. Babareko, S.A. Vladimirov, and I.V. Egiz, *Teoriya obrazovaniya tekstur v metallakh* [The theory of formation of textures in metals] (Moscow: Nauka: 1979) (in Russian).
164. S.V. Dobatkin, P.D. Odessky, and S.V. Shagalina, *Mat. Sci. Forum*, **584–586**: 623 (2008). https://doi.org/10.4028/www.scientific.net/MSF.584-586.623
165. A.M. Glezer and L.S. Metlov, *Fiz. Tverd. Tela*, **6**: 1090 (2010) (in Russian).
166. S.A. Firstov, V.F. Gorban', E.P. Pechkovskiy, and N.A. Mameka, *Sbornik Dokladov Khar'kovskoi Nanotekhnologicheskoi Assamblei*, **1**: 52 (2007) (in Russian).
167. V. Randle and O. Engler, *Introduction to Texture Analysis: Macrotexture, Microtexture and Orientation Mapping* (London: CRC Press: 2000).
168. V.F. Gorban', E.P. Pechkovskiy, and S.A. Firstov, *Metallofiz. Noveishie Tekhnol.*, **28**, No. 1: 67 (2006) (in Russian).
169. V.F. Gorban', E.P. Pechkovskiy, and S.A. Firstov, *Elektronnaya Mikroskopiya i Prochnost' Materialov*, **15**: 89 (2008) (in Russian).
170. Cheng Yang-Tse and Cheng Che-Min, *Appl. Phys. Lett.*, **73**, No. 5: (1998). https://doi.org/10.1063/1.121873
171. B.A. Galanov and O.N. Grigor'ev, *Elektronnaya Mikroskopiya i Prochnost' Materialov*, No. 13: 4 (2006) (in Russian).
172. M.L. Trunov, V.S. Bilanich, and S.N. Dub, *ZhTF*, **77**, No. 10: (2007) (in Russian).
173. S.N. Dub, O.N. Grigoryev, and O.V. Sobol, *Functional Materials*, **13**, No. 1: 105 (2006).
174. D.B. Shtansky, S.A. Kulinich, and E.A. Levashov, *Thin Solid Films*, **420**: 330 (2002). https://doi.org/10.1016/S0040-6090(02)00942-2
175. C.J. McHargue, *Thin Solid Films*, 162: 363 (1988). https://doi.org/10.1007/978-1-4684-5967-8_23
176. O.N. Grigor'ev, *Poroshkovaya Metallurgiya*, 1: 74 (1982) (in Russian).
177. V.I. Trefilov, Yu.V. Milman, and I.V. Gridneva, *Crys. Res. Technol.*, **19**, No. 3: 413 (1984). https://doi.org/10.1002/crat.2170190321
178. O.B. Perevalova and A.V. Panin, *Proc. Symp. 'Environments with structural and magnetic ordering'* (Rostov-na-Donu, September 4–8, 2011), p. 112 (in Russian).
179. Yu.V. Milman, S.I. Chugunova, I.V. Goncharova, and A.A. Golubenko, *Usp. Fiz. Met.*, **19**, No. 3: 271 (2018). https://doi.org/10.15407/ufm.19.03.271
180. Yu.V. Mil'man, S.I. Chugunova, and I.V. Goncharova, *Issledovanie mekhanicheskogo povedeniya maloplastichnykh materialov metodom indentirovaniya* [The investigation of the mechanical behaviour of low-plastic materials] (Tomsk: Izdatel'stvo NTL: 2006) (in Russian).
181. Yu.V. Milman and I.V. Goncharova, *Usp. Fiz. Met.*, **18**, No. 3: 265 (2017) (in Russian). https://doi.org/10.15407/ufm.18.03.265
182. A.N. Orlov and V.R. Regel', Plastichnost'. *Fizicheskiy entsiklopedicheskiy slovar'* [The plasticity. Physical Thesaurus] (Moscow: Sovetskaya entsiklopediya: 1965) (in Russian).
183. A.I. Yurkova, Yu.V. Mil'man, and A.V. Byakova, *Deformatsiya i Razrushenie Materialov*, **2**: 2 (2009) (in Russian).
184. Yu.V. Milman, B.A. Galanov, and S.I. Chugunova, *Acta Met. Mater.*, **41**, No. 9: 2523 (1993). https://doi.org/10.1016/0956-7151(93)90122-9

185. Yu.V. Milman, W. Lojkowski, S.I. Chugunova, D.V. Lotsko, I.V. Gridneva, and A.A. Golubenko, *Solid State Phenom.*, **94**: 55 (2003). https://doi.org/10.4028/www.scientific.net/SSP.94.55
186. V.Z. Kutsova and G.P. Stetsenko, *Metaloznavstvo ta Termichna Obrobka Metaliv*, **2**: 55 (2016) (in Russian).

Received October 24, 2018;
in final version, January 13, 2019

Ю.С. Пройдак, В.З. Куцова, Т.В. Котова,
Г.П. Стеценко, В.В. Прутчикова
Національна металургійна академія України,
пр. Гагаріна, 4, 49000 Дніпро, Україна

ЗАКОНОМІРНОСТІ ФОРМУВАННЯ СТРУКТУРИ, ТЕКСТУРИ ТА ВЛАСТИВОСТЕЙ ПРИ КОМБІНОВАНІЙ ПЛАСТИЧНІЙ ДЕФОРМАЦІЇ НИЗЬКО- Й УЛЬТРАНИЗЬКОВУГЛЕЦЕВИХ СТАЛЕЙ ДЛЯ ХОЛОДНОГО ШТАМПУВАННЯ

У роботі одержано нові розв'язки науково-практичної задачі, яка полягає у підвищенні комплексу механічних властивостей і схильности до штампування гарячевальцьованих низько- та ультранизьковуглецевих сталей з подальшою холодною деформацією методами осаду та кручення під гідростатичним тиском (КГТ). За допомогою сучасних метод дослідження встановлено можливість формування ультрадрібнокристалічної структури при комбінованій пластичній деформації. Встановлено залежність зміни механічних властивостей від параметрів структури, текстури та фазового складу. Вперше методом наноіндентування визначено механічні характеристики гарячевальцьованих сталей 08пс, 01ЮТ, 01ЮТ (Са), 01ЮТА з подальшою холодною деформацією методом КГТ. Встановлено підвищення в 2 рази твердости індентування (5,5–6,0 ГПа), пониження модуля пружности в 1,5 рази (150–190 ГПа) та збереження задовільної пластичности (δ = 0,75–0,8), що ґарантовано забезпечує більшу схильність до штампування досліджених сталей порівняно з гарячевальцьованим станом.

Ключові слова: ультранизьковуглецеві сталі, наноіндентування, інтенсивна пластична деформація, кручення під гідростатичним тиском, штампування, текстура.

Ю.С. Пройдак, В.З. Куцова, Т.В. Котова,
А.П. Стеценко, В.В. Прутчикова
Национальная металлургическая академия Украины,
пр. Гагарина, 4, 49000 Днепр, Украина

ЗАКОНОМЕРНОСТИ ФОРМИРОВАНИЯ СТРУКТУРЫ, ТЕКСТУРЫ И СВОЙСТВ ПРИ КОМБИНИРОВАННОЙ ПЛАСТИЧЕСКОЙ ДЕФОРМАЦИИ НИЗКО- И УЛЬТРАНИЗКОУГЛЕРОДИСТЫХ СТАЛЕЙ ДЛЯ ХОЛОДНОЙ ШТАМПОВКИ

В работе получены новые решения научно-практической задачи, которая заключается в повышении комплекса механических свойств и склонности к штамповке горячекатаных низко- и ультранизкоуглеродистых сталей с последующей холодной деформацией методами осадки и кручения под гидростатическим давлением (КГД). С помощью современных методов исследования установлена возможность формирования ультрамелкокристаллической структуры при комбинированной

пластической деформации. Установлена зависимость изменения механических свойств от параметров структуры, текстуры и фазового состава. Впервые методом наноиндентирования определены механические характеристики горячекатаных сталей 08пс, 01ЮТ, 01ЮТ(Са), 01ЮТА с последующей холодной деформацией методом КГД. Установлено повышение в 2 раза твёрдости индентирования (5,5–6,0 ГПа), снижение модуля упругости в 1,5 раза (150–190 ГПа) и сохранение удовлетворительной пластичности (δ = 0,75–0,8), что гарантированно обеспечивает большую склонность к штамповке исследуемых сталей по сравнению с горячекатаным состоянием.

Ключевые слова: ультранизкоуглеродистые стали, наноиндентирование, интенсивная пластическая деформация, кручение под гидростатическим давлением, штамповка, текстура.